Journal of Materials Chemistry B

ROYAL SOCIETY OF CHEMISTRY

PAPER

View Article Online
View Journal

Cite this: DOI: 10.1039/d6tb00121a

Poly(glutamic acid-*block*-tyrosine) peptides designed for gastrointestinal drug adsorption

Hunter B. Wood, [a] Joseph T. Dosch,†[a] Stella M. Trickett,†[a] Juhi Singh,[a] Farin M. Weinger,[a] Gerald J. Wang, [b] Dazhe J. Cao[c] and Stefanie A. Sydlik *[ad]

Received 16th January 2026,
Accepted 13th May 2026

DOI: 10.1039/d6tb00121a

rsc.li/materials-b

Drug overdose remains a major public health challenge, particularly for non-opioid substances that lack effective antidotes and are often treated through gastrointestinal decontamination with activated charcoal. While activated charcoal is broadly effective, its use is associated with aspiration risks and gastrointestinal complications. Here, we report a class of synthetic poly(glutamic acid-*block*-tyrosine) (EY) peptide adsorbent materials designed as biocompatible, tuneable alternatives for gastrointestinal drug adsorption. EY polypeptides were synthesized *via* *N*-carboxyanhydride ring-opening polymerization with systematically varied tyrosine block lengths to investigate how amino acid composition and length govern adsorption. Adsorption kinetics and capacity were evaluated under simulated gastric (pH 1.2) and intestinal (pH 6.8) conditions for clinically relevant drugs commonly implicated in overdose: amitriptyline (AMI), bupropion (BUP), hydroxychloroquine (HCQ), and strychnine (STR). Increasing tyrosine content enhanced drug uptake, with the top-performing formulation (E30Y129) achieving high adsorption capacities and binding affinities comparable to reported adsorbent biopolymers and competitive with activated charcoal for certain drugs. Langmuir isotherm analysis revealed maximum adsorption capacities of 40–238 mg g^{-1} and binding affinities up to 0.214 L g^{-1}, with adsorption behavior dependent on drug characteristics. Exploratory fed-state experiments demonstrated that adsorbent properties are retained in the presence of a complex nutrient matrix and vary depending on drug properties. Preliminary enzyme degradation studies indicated gradual proteolysis under gastrointestinal conditions, and cytocompatibility assays with fibroblasts and macrophages showed no overt toxicity across relevant concentrations. Collectively, these results demonstrate that synthetic polypeptides can be engineered to achieve efficient, clinically relevant drug adsorption while offering advantages in biocompatibility, degradability, and tunability. This work establishes a foundation for next-generation gastrointestinal decontamination materials beyond activated charcoal.

Introduction

Accidental drug overdose deaths increased nearly four-fold for both men and women between 2000 and 2020.[1] Further, between January 2020 to January 2021, drug overdose death rates rose by a staggering 26.4%, coinciding with the beginning of the COVID-19 pandemic.[2] Although opioids account for many of these deaths, a substantial number involve non-opioid substances.[3] Opioid overdose can be effectively reversed using naloxone if administered with multiple doses as necessary. However, most non-opioids do not have drug-specific antidotes in cases of overdose. When an oral overdose involves a drug without a specific antidote, treatment may include gastrointestinal decontamination with activated charcoal (AC) to bind the drug before systemic absorption occurs.[4]

AC is the clinical standard for gastrointestinal decontamination due to its chemical structure that facilitates adsorption through various intermolecular interactions. There is a large delocalized network of π-electrons associated with the carbon surface of AC.[5] This high π-electron density promotes the adsorption of drugs to AC through π–π and hydrophobic interactions.[5,6] The large specific surface area of AC encourages drug loading in this manner, as it provides an enormous space for these interactions with adsorbates to occur.[7]

The honeycomb lattice framework of AC further promotes adsorption by conferring porosity to the material. Pores provide internal free volume to AC, increasing the specific surface area

[a] Department of Chemistry, Carnegie Mellon University, 4400 Fifth Avenue, Pittsburgh, PA, USA. E-mail: ssydlik@andrew.cmu.edu
[b] Department of Civil and Environmental Engineering, Carnegie Mellon University, 5000 Forbes Avenue, Pittsburgh, PA, USA
[c] Department of Emergency Medicine, University of Texas Southwestern Medical Center, Dallas, TX, USA
[d] Department of Biomedical Engineering, Carnegie Mellon University, 5000 Forbes Avenue, Pittsburgh, PA, USA
† These authors contributed equally.

of the material and facilitating drug adsorption through greater solvent penetration.[8] AC also interacts with adsorbates *via* oxygen-containing functional groups, rendering it a highly versatile adsorbent.[9] Aside from its physical and chemical properties, AC is ideal for commercial use because it is inexpensive and can be prepared from a variety of waste products.[10]

AC is also widely considered to be nontoxic, and is expelled through normal digestive processes following ingestion.[11] However, drug overdose treatment using AC still involves risk. Administration of AC poses an aspiration hazard due to its unpalatable flavor, and emesis may occur leading to further complications.[11] When AC enters the lungs, it can result in a variety of respiratory issues.[12] Fatalities have even been reported in severe cases of pulmonary AC aspiration.[11,13,14] Risk of pulmonary aspiration is also high for patients presenting with central nervous system depression and altered mental status, which complicates the emergency treatment of drug overdose using AC.[11] Aside from respiratory concerns, gastrointestinal complications (including bowel obstructions) have also been reported following overdose treatment using AC, and medical intervention is sometimes required.[11,15–17]

The limitations associated with AC motivate the development of alternative adsorbent materials for gastrointestinal drug adsorption. Synthetic polypeptides represent a promising platform because they can be designed to exhibit favorable biocompatibility and degradation profiles.[18] Synthetic polypeptides resemble biological macromolecules more closely than AC, making them attractive for applications where cytocompatibility is an important consideration.[19] Peptide backbones are also susceptible to enzymatic degradation, allowing degradation behavior to be incorporated as a material design element.[20] Beyond biological considerations, synthetic polypeptides offer substantial chemical tunability, enabling adsorbent properties to be tailored through polymer composition.[21] The primary structure of the polypeptide influences adsorption through intermolecular interactions that can occur between the adsorbates and amino acid residues.[22] Higher-order organization, including secondary structure and self-assembled aggregate morphology, can also influence adsorption by controlling the orientation, density, and accessibility of functional groups at the material-solution interface.[22–24]

We previously reported a class of polypeptide adsorbent materials (KEYs) designed for gastrointestinal drug adsorption.[25] This platform demonstrated that triblock copolypeptides formulated with lysine, glutamic acid, and tyrosine can combine pH-responsive electrostatic interactions, π–π interactions, hydrophobic interactions, and hydrogen bonding, to achieve strong adsorption of small molecules under simulated gastrointestinal conditions. While that study demonstrated the capability of polypeptides as tunable adsorbent materials, it did not comprehensively investigate the role of amino acid composition and polymer block length on adsorption performance.

In this study, we developed a class of poly(glutamic acid-*block*-tyrosine) peptides to investigate how amino acid composition and block length influence drug adsorption. Using the highest-performing formulation, we then evaluated adsorption behavior through isotherm modeling. While this work focuses on proof-of-concept, it also expands on existing research by examining factors relevant to gastrointestinal applications, including fed *versus* fasted-state drug adsorption, stability toward certain gastrointestinal enzymes, and preliminary cytocompatibility with mammalian cells. This research demonstrates that polypeptides can be engineered for efficient drug adsorption under simulated gastrointestinal conditions and supports their further investigation as tunable biomaterial adsorbents.

Experimental

Materials

Protected amino acids (γ-benzyl-L-glutamate and *O*-benzyl-L-tyrosine) and triphosgene were purchased from commercial suppliers and used for *N*-carboxyanhydride (NCA) synthesis without further purification. Common organic solvents and reagents were obtained from standard vendors and purified as required for moisture-sensitive reactions. Deuterated solvents for proton nuclear magnetic resonance (^{1}H NMR) analysis were also commercially sourced. Simulated gastric fluid (SGF) and simulated intestinal fluid (SIF), with and without digestive enzymes, were prepared according to United States Pharmacopeia guidelines or literature precedent. RAW 264.7 murine macrophages and NIH 3T3 fibroblasts were maintained in Dulbecco's modified eagle medium supplemented with fetal bovine serum and antibiotics under standard cell culture conditions. Full preparation details are provided in the SI.

Synthesis

Poly(glutamic acid-*block*-tyrosine) peptides were synthesized *via* sequential ring-opening polymerization of amino acid *N*-carboxyanhydrides (NCAs). Protected γ-benzyl-L-glutamate and *O*-benzyl-L-tyrosine NCAs were prepared using triphosgene and polymerized under inert atmosphere using hexylamine initiation to generate a poly(glutamic acid) macroinitiator, followed by chain extension with tyrosine NCAs to yield block copolymers with systematically varied tyrosine block lengths. Following polymerization, benzyl protecting groups were removed using acid-mediated deprotection to obtain partially ionized poly(glutamic acid-*block*-tyrosine) materials. Polymers were purified by repeated dissolution and precipitation, followed by dialysis against deionized water, and isolated as lyophilized powders. Full synthetic procedures and characterization are provided in the SI.

Characterization

Polypeptide structure and composition were confirmed using Fourier transform infrared spectroscopy (FTIR) and ^{1}H NMR. Particle size distributions and surface charge were measured by dynamic light scattering (DLS) and zeta potential analysis in simulated gastric and intestinal fluids. Particle morphology and aggregation behavior were evaluated using scanning electron microscopy (SEM) and optical microscopy. Drug

concentrations in adsorption experiments were quantified by ultraviolet-visible (UV-Vis) absorbance using experimentally determined wavelengths and calibration curves. Full characterization methods and parameters are provided in the SI.

Adsorption kinetics and capacity

Adsorption kinetics and equilibrium capacity were evaluated using batch adsorption experiments conducted at 37 °C. Drug solutions and polypeptide suspensions were combined at fixed adsorbent (polypeptide)-to-adsorbate (drug) mass ratios appropriate for kinetic (10 : 1) or capacity (13 : 1) measurements and incubated with rotational mixing. Drug solutions were soluble while polypeptide suspensions were milky white, with visible insoluble particles. At predetermined time points, polypeptides were filtered from solution using centrifugal filter units of molecular weight cutoff (MWCO) 3 kDa, and the concentration of unbound drug in the supernatant was quantified. The adsorption equilibration time was defined as the point at which no further change in percent adsorption was observed. Detailed experimental conditions are provided in the SI.

Adsorption isotherm modeling

In a typical adsorption isotherm experiment, drug and polypeptide mixtures were prepared separately in 20 mL scintillation vials. Drug solutions were soluble while polypeptide suspensions were milky white, with visible insoluble particles. To prepare the experimental samples, the drug solution was added to an Eppendorf tube. Next, a dispersion of polypeptide in buffer was added to each Eppendorf to give adsorbent-to-adsorbate mass ratios typically ranging from 0.25 : 1 to 20 : 1. All experimental samples were prepared with the same final volume. The Eppendorf tubes were vortexed briefly to mix and incubated at 37 °C with rotational shaking. After incubating for the equilibration time (determined from adsorption kinetics experiments), the Eppendorf tubes were removed from the incubator, centrifuged using filter units (MWCO 3 kDa), and the supernatant was plated and analyzed. More detail on the experimental conditions used for these studies may be found in the SI.

Cell culture

Cytocompatibility of the polypeptide materials was evaluated in RAW 264.7 macrophages and NIH 3T3 fibroblasts using a fluorescence-based viability assay. Cells were exposed to materials at concentrations of 1–250 μg mL^{-1} for 48 h, followed by assessment of total cell number, viability, and membrane integrity using Hoechst 33342, Calcein acetoxymethyl ester (AM), and propidium iodide, respectively. Fluorescence measurements were complemented by direct fluorescence imaging to account for potential interference from polypeptide particulates. Full experimental details are provided in the SI.

Statistical analysis

For adsorption studies, data are reported as mean ± standard deviation, with error bars representing one standard deviation computed over independent, triplicate measurements. Statistical significance was determined separately for each drug within each medium by one-way analysis of variance (ANOVA) followed by Tukey's *post hoc* test. For cell culture studies, five independent measurements were performed for each condition. Statistical significance was assessed using one-way ANOVA followed by Dunnett's *post hoc* test for multiple comparisons relative to control conditions. For all analyses, statistical significance is denoted as follows: $p < 0.05$ (*), $p < 0.01$ (**), $p < 0.001$ (***), and ns = not significant.

Results and discussion

Experimental design considerations

The library of poly(glutamic acid-*block*-tyrosine) peptides prepared and studied in this manuscript were developed using "E" (glutamic acid) and "Y" (tyrosine) amino acids and are aptly referred to as "EY" polypeptides (EYs). This study extends our prior work on "KEY" polypeptide adsorbents, which incorporated lysine, glutamic acid, and tyrosine in a different amino acid composition than the EYs investigated in this work.[25] While highly effective for certain small molecules, the adsorption profile of KEYs suggested the need for a complementary design better suited to drugs commonly overdosed in the United States. KEYs have positively charged polylysine residues which have a high affinity for negatively charged groups. However, many commonly overdosed drugs are weak bases that carry a positive charge at physiological pH.[26,27] EYs were rationally designed to optimize the adsorption of these drugs, by omitting lysine from the formulation.

Since the pK_a of the glutamic acid side chain is roughly 4.1, the residue will be negatively charged in intestinal fluid (pH 6.8).[28] This encourages adsorption through attractive interactions between the negatively charged side chain and the positively charged drug (Fig. 1). In simulated gastric fluid (pH 1.2), the glutamic acid side chain will be protonated, but can still adsorb drugs through weaker, hydrogen bonding interactions (Fig. 1).[28] However, the contribution of hydrogen bonding can be attenuated in aqueous environments because water molecules can occupy or hinder access to hydrogen-bonding adsorption sites.[29] Further, since our previous work suggested that local salt concentrations may interfere with electrostatic interactions between the side chain and drug, π-stacking interactions were prioritized for the purpose of optimizing the polypeptides for drug adsorption.[25]

As such, the length of the tyrosine block in the polypeptide formulation was explored to determine the degree to which drug adsorption was promoted through π–π or hydrophobic interactions between the phenolic side chain and aromatic drugs. In this study, block copolypeptides E30Y28, E30Y79, E30Y101, and E30Y129 were prepared to probe the impact of this effect on adsorption, where the number following each amino acid moniker represents the degree of polymerization for each block in the copolypeptide. The series of polypeptides were prepared using the same E30 macroinitiator and therefore share the same E30 block. Polymer lengths were targeted to

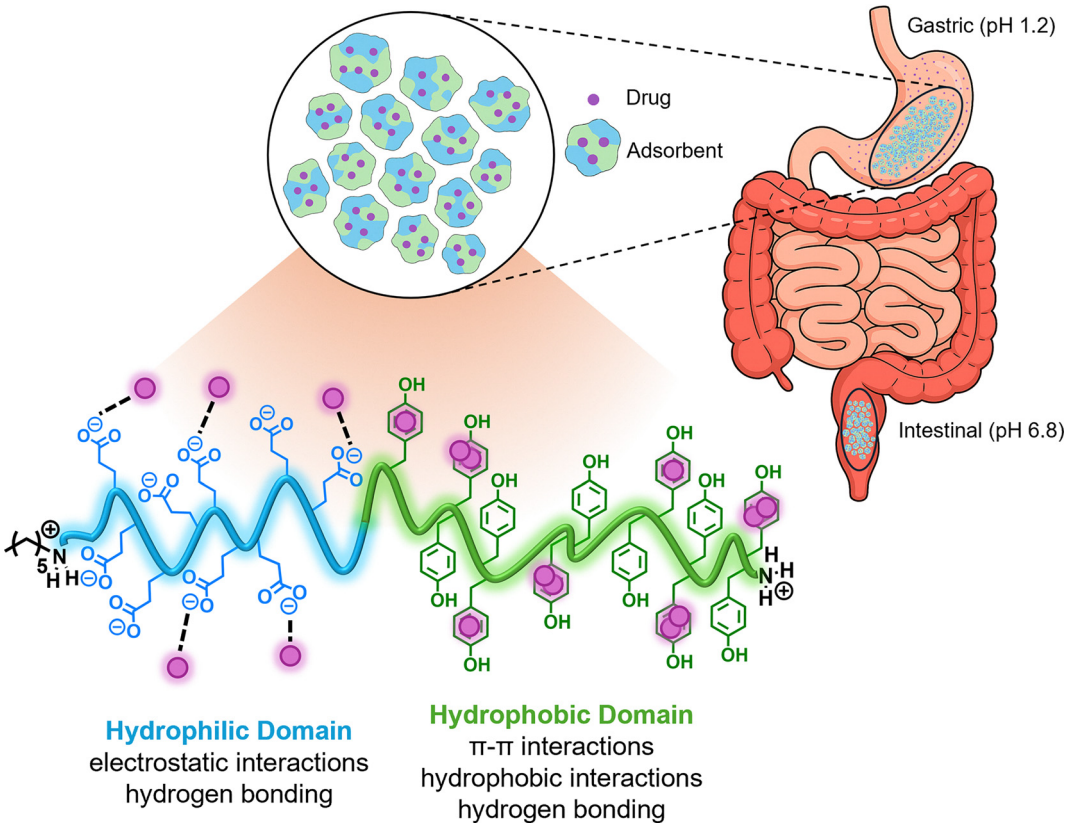

Fig. 1 Proposed function of poly(glutamic acid-*block*-tyrosine) peptides (EYs) for gastrointestinal drug adsorption. The schematic illustrates an amphiphilic polypeptide containing a glutamic acid rich hydrophilic domain and a tyrosine rich hydrophobic domain, which can form adsorbent particles in gastric and intestinal environments. Purple circles represent drug molecules. Glutamic acid residues provide ionizable groups that can contribute to electrostatic interactions and hydrogen bonding, while tyrosine residues provide aromatic and hydrophobic groups that can contribute to π–π interactions, hydrophobic interactions, and hydrogen bonding. The interactions shown represent proposed noncovalent contributors to adsorption and are not intended to imply a single binding mode for all drugs or media.

remain within the range accessible by conventional, catalyst-free, primary amine-initiated *N*-carboxyanhydride (NCA) ring-opening polymerization (ROP).[30] To encourage the formation of aggregates through hydrophobic collapse in aqueous conditions, glutamic acid (hydrophilic) and tyrosine (hydrophobic) were also synthesized as separate blocks.[31]

Characterization

L-α-amino acid *N*-carboxyanhydride (NCA) monomers were prepared from protected amino acids using triphosgene (Fig. S1 and S2). EYs were polymerized from NCA monomers *via* ring-opening polymerization (ROP) using hexylamine as the initiator. Hexylamine was first added to a solution of E-NCA dissolved in dry *N*,*N*-dimethyl formamide (DMF) to prepare a poly(glutamic acid) macroinitiator (pE30). Once Fourier-transform infrared (FTIR) spectroscopy had indicated the depletion of the E-NCA monomer through the absence of the anhydride peak, accurate volumes of the E30 macroinitiator were transferred to different solutions of Y-NCA to prepare EY polypeptides with the same lengths of the glutamic acid block, but varying tyrosine block lengths. The resulting reactions were monitored for conversion using FTIR, and precipitated from solution following consumption of the anhydride. Polypeptides were deprotected according to standard acidic deprotection procedures.[32–34] Following dialysis against deionized water, the polypeptides were characterized to ensure proper synthesis and deprotection. Full synthetic details can be found in the SI.

The Fourier-transform infrared (FTIR) spectra of the EYs display the characteristic signatures of both the peptide backbone and the constituent amino acid side chains, with clear compositional trends as tyrosine incorporation increases from E30Y28 to E30Y129 (Fig. 2A). The backbone is defined by the amide A band at ∼3200–3400 cm^{-1},[35] amide I band at ∼1640 cm^{-1},[35] arising primarily from C=O stretching, the amide II band at ∼1534 cm^{-1} from N–H bending and C–N stretching,[35] and the amide III band at ∼1238 cm^{-1}.[35] Glutamic acid side-chain contributions are also evident, including CH_2 bending at ∼1444 cm^{-1}, C–C/N–C stretching at ∼1116 cm^{-1}, and COOH deformation near ∼624 cm^{-1}.[36] Signals corresponding to tyrosine are also present at ∼1514 cm^{-1} (aromatic C–C ring), ∼1444 cm^{-1} (CH_2 bending, overlapping with glutamate), ∼1176 cm^{-1} (C–H ring bending), ∼1018 cm^{-1} (aromatic C–C ring), ∼842 and ∼824 cm^{-1} (Fermi doublet of the phenolic ring), ∼736 and ∼698 cm^{-1} (aromatic C–H out-of-plane bending), and ∼624 cm^{-1} (out-of-plane ring

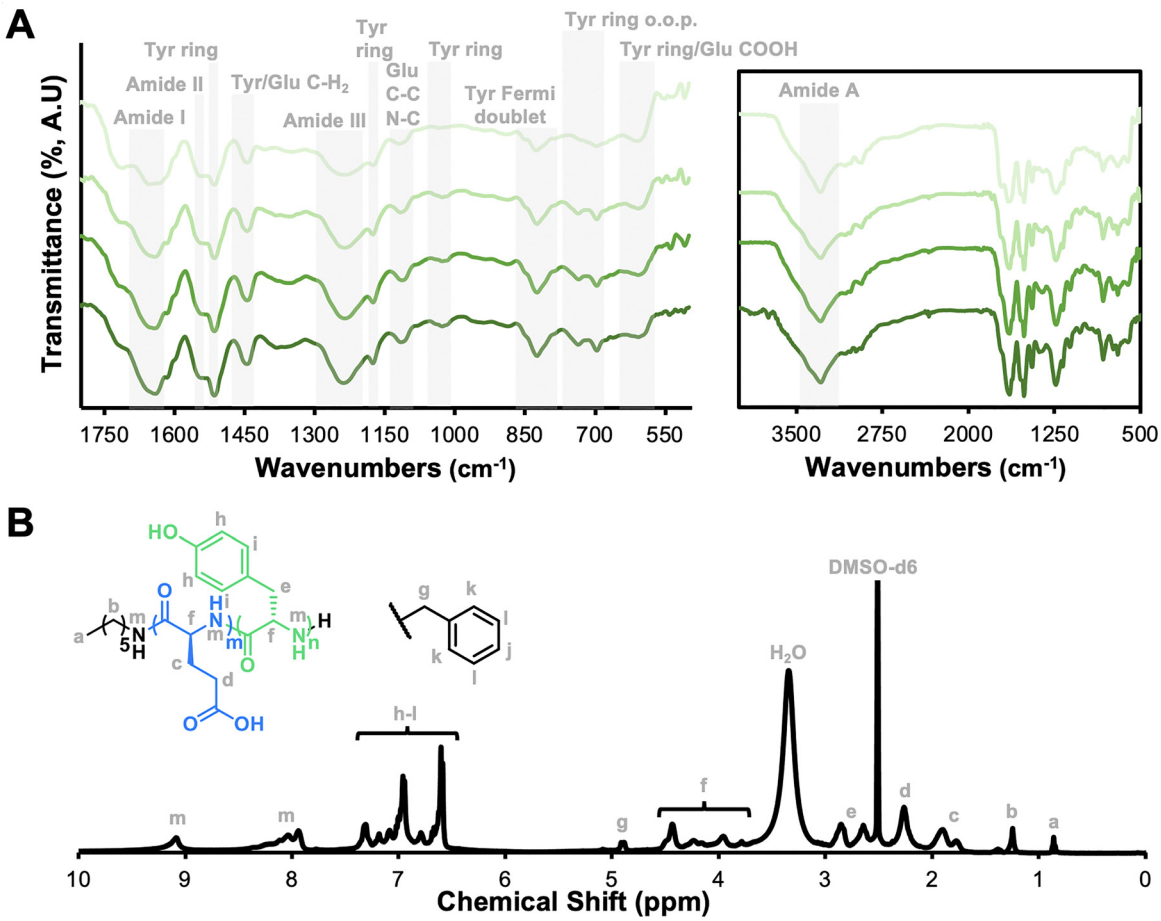

C

Synthetic Target	Target MW (kDa)	^{1}H NMR M_n (kDa)	DP E	DP Y
p(E30) macroinitiator	6.7	6.7	30	
p(E30-block-Y30)	14.3	13.8	30	28
p(E30-block-Y75)	25.7	26.6	30	79
p(E30-block-Y100)	32.0	32.2	30	101
p(E30-block-Y125)	38.3	39.4	30	129

Fig. 2 Structural characterization of poly(glutamic acid-*block*-tyrosine) peptides (EYs). (A) gives Fourier transform infrared spectroscopy (FTIR) spectra for the E30 macroinitiator and EYs, with annotated backbone and side chain vibrations from glutamic acid and tyrosine. The inset shows the full spectral range, including the amide A region. (B) Shows a representative proton nuclear magnetic resonance (^{1}H NMR) spectrum of E30Y28 with assignments used for end group analysis. (C) Provides synthetic targets, target molecular weights (MW), ^{1}H NMR determined number average molecular weights (M_n), and calculated glutamic acid and tyrosine degrees of polymerization (DP) for the E30 macroinitiator and EYs. Color-coding presents the E30 macroinitiator and glutamic acid block as blue, with the EYs presented as increasingly dark green based on increasing tyrosine block length.

deformation, overlapping with glutamate).[36] A progressive increase in intensity is observed with higher tyrosine incorporation: specifically, the aromatic C–C vibration at ~1514 cm^{-1}, the C–H in-plane bending at ~1176 cm^{-1}, the aromatic skeletal vibration at ~1018 cm^{-1}, the diagnostic Fermi doublet at ~842/824 cm^{-1}, and the out-of-plane C–H bending modes at ~736/698 cm^{-1}.[36] The evolution of these features suggests the successful and progressive incorporation of tyrosine into the copolypeptide series, as signal intensity is proportional to functional group density.

Weight-average molecular weight and dispersity could not be reliably evaluated for the EY series because of limited solubility under the available gel permeation chromatography (GPC) conditions. Instead, proton nuclear magnetic resonance spectroscopy (^{1}H NMR) was used to determine the number-average molecular weight (M_n) and degree of polymerization (DP) of the polypeptides (Fig. 2B and C and Fig. S3–S11). Quantitative end-group analysis was performed by referencing the spectrum to the methyl signal of the hexylamine initiator. The aromatic region was used to determine DP and M_n because

these signals were well resolved and displayed consistent chemical shifts across solvents and between protected and deprotected forms. Following deprotection and purification, the integral of the remaining benzyl protecting-group signal was used to quantify the extent of deprotection (Fig. S5, S7, S9 and S11). The molecular weights and DPs were in good agreement with theoretical values, and near complete deprotection ($\geq$95%) was observed for all polypeptides.

Zeta potential measurements indicate changes in material properties with increasing chain length (Fig. 3A and B). These measurements were performed using dynamic light scattering (DLS) at 50 μg mL^{-1} to minimize concentration-dependent artifacts, including multiple scattering, particle–particle interactions, and preferential detection of strongly scattering aggregate populations.[37–40] These data are therefore used as comparative descriptors of formulation behavior rather than absolute measurements of aggregation state at the higher concentrations used during adsorption experiments. At pH 1.2, the zeta potential decreased from 8.3 mV (E30Y28) to 3.7 mV (E30Y129), while at pH 6.8, it increased from −29.3 mV (E30Y28) to −22.3 mV (E30Y129) (Fig. 2E). This trend may reflect tyrosine-driven changes in aggregate organization, where increasing hydrophobic tyrosine content alters the exposure of ionizable glutamic acid residues at the particle–solution interface. Reduced presentation of glutamate carboxylates at the aggregate surface would decrease the effective interfacial charge density, consistent with the lower positive zeta potential in SGF and less negative zeta potential in SIF as tyrosine block length increases.[41]

To better characterize the EYs under hydrated conditions, polypeptide suspensions were also prepared at 1 mg mL^{-1} in SIF and studied using low-magnification microscopy at 10× and 20× (Fig. 3C, 10× and 20×). At low tyrosine content (E30Y28), the suspension was sparse and featured a limited number of insoluble particles. However, as tyrosine content increased, the EY suspensions became progressively denser with more apparent aggregation. This is consistent with increased hydrophobicity at higher tyrosine content, leading to aggregation *via* hydrophobic collapse in aqueous media. Microscopy of polypeptide suspensions in SGF was not performed since dynamic light scattering (DLS) measurements indicated similar particle size distributions for all formulations under acidic conditions (Fig. S12–S15).

EY polypeptides were also examined by scanning electron microscopy (SEM) to qualitatively assess how variations in amino acid composition affect microstructural features (Fig. 3C, 1000× and 3000×). Although SEM appearances can be influenced by sample preparation, all materials were prepared identically, enabling meaningful side-by-side comparison. High-magnification SEM imaging (1000× and 3000×) revealed clear morphological trends with increasing tyrosine content among the EYs. E30Y28 featured a relatively smooth surface with little texture, indicative of a more cohesive bulk morphology. In contrast, E30Y79, E30Y101, and E30Y129 exhibited progressively textured morphologies with apparent microdomains. Collectively, these observations suggest a gradual shift from compact, smooth particles at low tyrosine content to increasingly heterogeneous morphologies at higher tyrosine content, which may influence dispersibility and accessibility of available sites for drug binding. However, because these observations are based on freeze-dried materials, surface morphology may differ under hydrated gastrointestinal conditions.

Adsorption kinetics

Following characterization, kinetics experiments were performed with commonly overdosed drugs to determine the rate of drug adsorption to the peptide amphiphiles. Our previous study found that KEYs had a low affinity for amitriptyline.[25] To determine whether EY polypeptides improved adsorption of similar drugs, materials were tested with amitriptyline (AMI), bupropion (BUP), hydroxychloroquine (HCQ), and strychnine (STR) (Fig. 4A). These compounds are associated with severe clinical toxicity in overdose, including rapid cardiovascular collapse (HCQ),[42] delayed-onset seizures (BUP),[43] and life-threatening arrhythmias (AMI),[44] as well as potent neurotoxicity (STR).[45] They encompass a range of geometries and physicochemical properties, and together reflect clinically relevant and challenging scenarios for gastrointestinal decontamination. Studying this panel provides a rigorous assessment of adsorbent performance across diverse toxins of medical significance.

E30Y129 was selected as a representative model for adsorption kinetics. Among the polypeptides examined, E30Y129 formed the cloudiest suspensions, consistent with extensive aggregation. Under diffusion-limited conditions when intraparticle mass transport governs uptake, aggregation is expected to slow diffusion to interior adsorption sites.[46,47] Accordingly, E30Y129 provides a conservative benchmark for evaluating adsorption kinetics. Experiments were conducted using a constant 10 : 1 adsorbent-to-adsorbate mass ratio in simulated gastric fluid (SGF, pH 1.2) or simulated intestinal fluid (SIF, pH 6.8). This ratio reflects a dose of activated charcoal that is generally used as a benchmark for gastrointestinal decontamination.[11] Similarly, SGF and SIF model the gastrointestinal environments relevant to the intended application of the polypeptides.[48] For each experiment, replicate samples of each drug/adsorbent mixture were incubated at 37 °C with rotational stirring. At defined time points, the sample was centrifuged using filter units with a molecular weight cutoff (MWCO) of 3 kDa to ensure soluble complexes and insoluble particles were removed from the supernatant. The amount of adsorbed compound was then quantified by measuring the concentration of free adsorbate in the supernatant *via* ultraviolet visible (UV-Vis) spectroscopy (Fig. S16–S23). Full experimental details can be found in the SI.

The kinetics experiments demonstrated that drug adsorption to the EYs is influenced by pH (Fig. S24–S27). The rate of drug adsorption is much slower in SGF (pH 1.2) compared to SIF (pH 6.8). At low pH, the timescale of drug adsorption is prolonged and adsorption does not generally plateau until 45 minutes of incubation (Fig. S24–S27A). However, at high pH, drug adsorption plateaus within the first 5 minutes of incubation for all drugs (Fig. S24B–S27B). This behavior

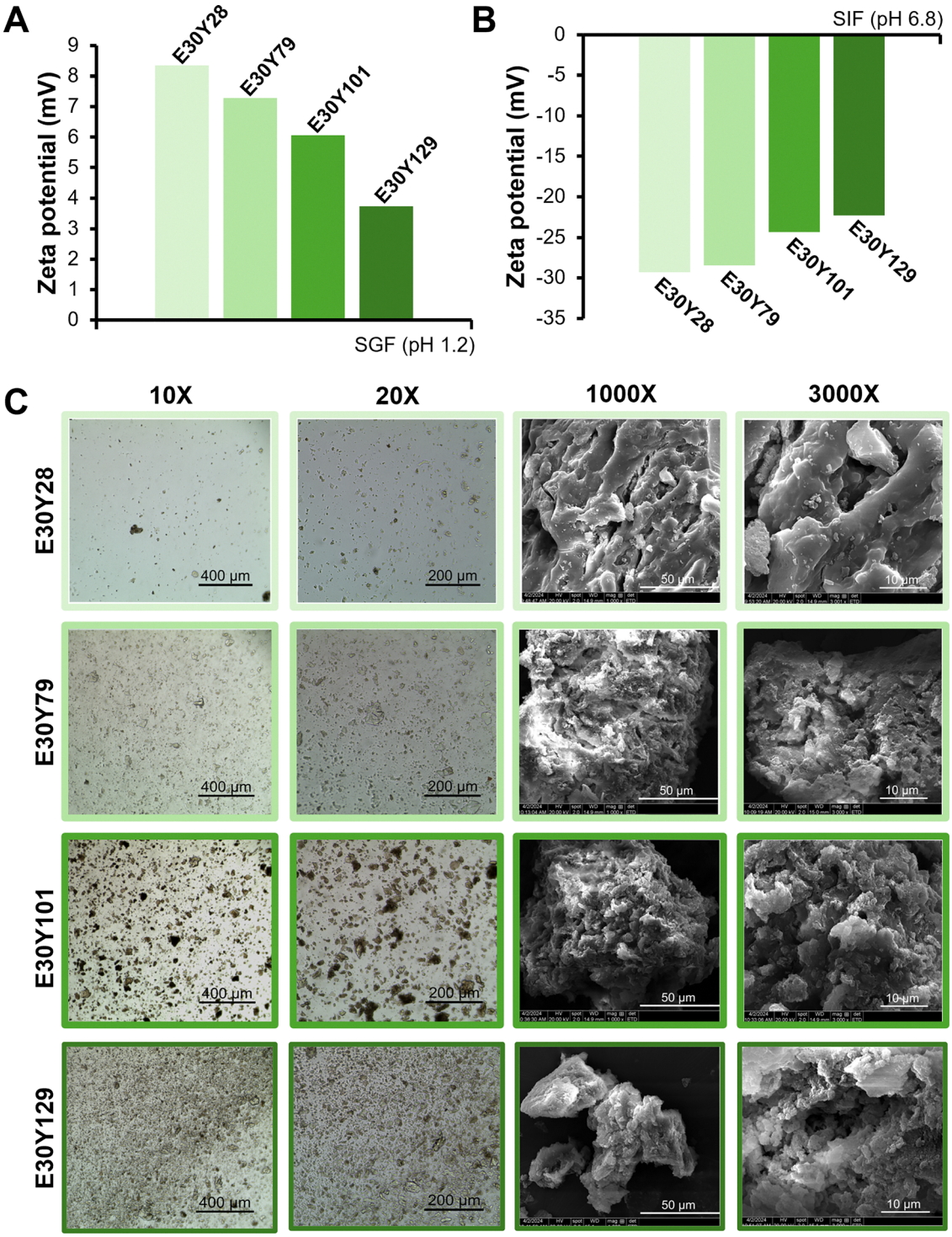

Fig. 3 Zeta potential (surface charge), solution-phase behavior, and dry-state surface morphology of poly(glutamic acid-*block*-tyrosine) peptides (EYs). A) gives zeta potential values for E30Y28, E30Y79, E30Y101, and E30Y129 in simulated gastric fluid (SGF, pH 1.2). (B) Gives zeta potential values for the same materials in simulated intestinal fluid (SIF, pH 6.8). Zeta potential measurements were performed at 50 µg mL^{-1} and are used as comparative descriptors of surface charge under dilute measurement conditions. (C) Shows optical microscopy images of EY suspensions in SIF at 10× and 20× magnification at 1 mg mL^{-1}, and scanning electron microscopy (SEM) images of lyophilized EY powders at 1000× and 3000× magnification. Transmitted light microscopy was used to compare hydrated aggregation behavior, while SEM was used to compare dry particle morphology. Scale bars are 400 µm for 10× magnification, 200 µm for 20× magnification, 50 µm for 1000× magnification and 10 µm for 3000× magnification. Color-coding presents the EYs as increasingly dark green based on increasing tyrosine block length.

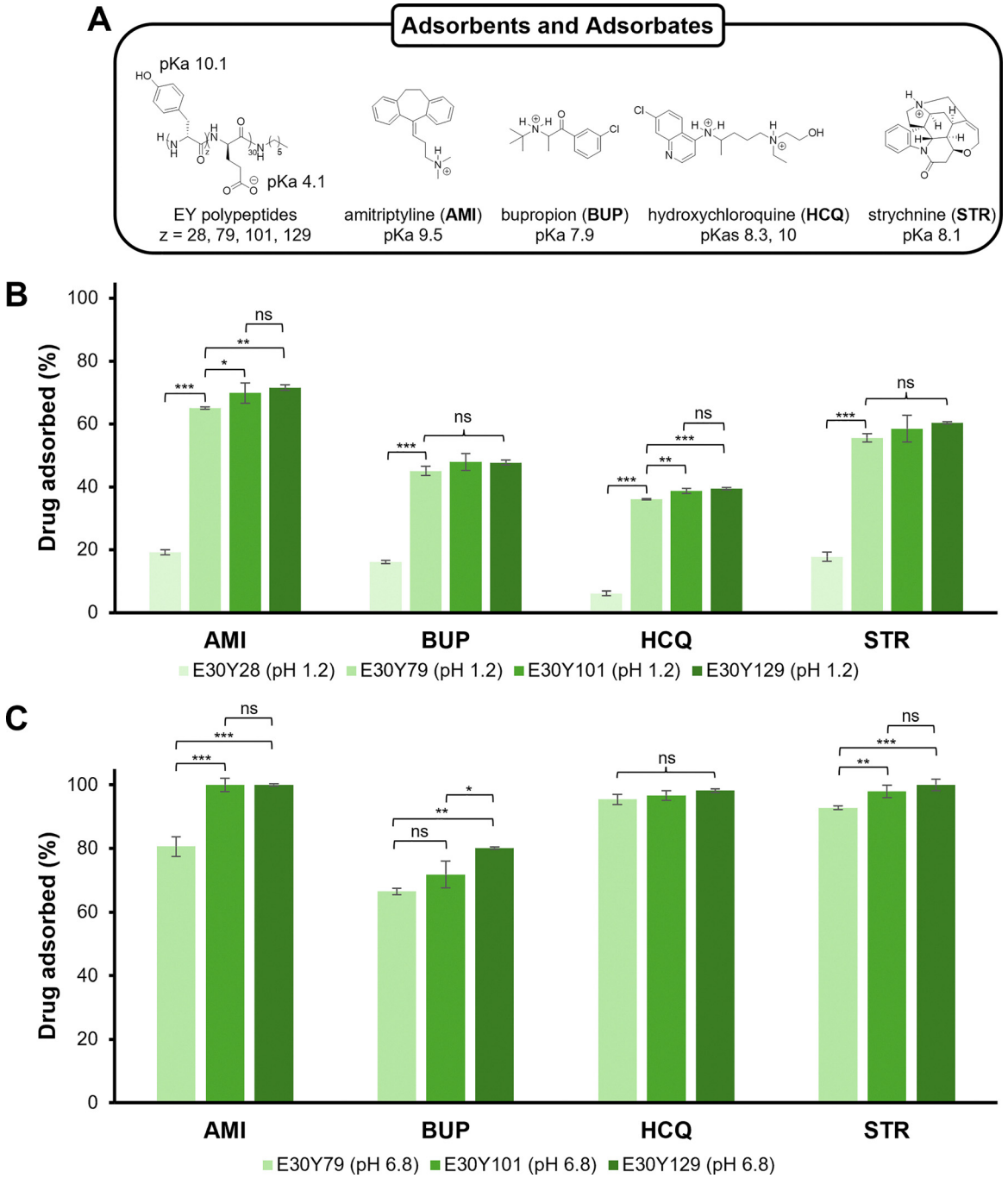

Fig. 4 Adsorption capacities of poly(glutamic acid-*block*-tyrosine) peptides (EYs) across a panel of clinically relevant adsorbates. (A) Shows the structures and pK_a values of the EYs and adsorbates evaluated in adsorption experiments, including amitriptyline (AMI), bupropion (BUP), hydroxychloroquine (HCQ), and strychnine (STR). (B) Shows percent drug adsorption to E30Y28, E30Y79, E30Y101, and E30Y129 in simulated gastric fluid (SGF, pH 1.2). (C) Shows percent drug adsorption to E30Y79, E30Y101, and E30Y129 in simulated intestinal fluid (SIF, pH 6.8). Adsorption experiments were performed at 37 °C using a 13 : 1 adsorbent-to-adsorbate mass ratio. E30Y28 was excluded from the primary SIF comparison because its colloidal and filter-passing behavior under SIF conditions complicated direct comparison with the more aggregated E30Y79, E30Y101, and E30Y129 materials. Data are shown as mean ± standard deviation from triplicate measurements. Statistical significance was determined separately for each drug within each medium by one way analysis of variance (ANOVA) followed by Tukey's *post hoc* test. Significance is denoted as * = $p < 0.05$, ** = $p < 0.01$, *** = $p < 0.001$, and ns = not significant.

suggests that drug adsorption to the EYs may occur through different mechanisms based on pH.

The rapid adsorption to the EYs at high pH is likely due to electrostatic attraction between positively charged drug molecules and negatively charged glutamic acid side chains. Below the glutamic acid side chain pK_a (4.1) however, carboxylic acids are protonated, and electrostatic interactions are broken. Considering the relative order of noncovalent interactions, this

difference in adsorption kinetics between simulated gastrointestinal media aligns with theoretical expectations. Electrostatic attraction is generally stronger than hydrogen bonding and π-stacking interactions.[49,50] When electrostatic attraction is not present, adsorption occurs more slowly because it proceeds *via* weaker interactions.[49,51] Because E30Y28 appeared visually consistent with a colloidally dispersed suspension in deionized water, it was expected to provide a more hydrated aggregate state with greater exposure of hydrophilic, ionizable glutamic acid residues at the aqueous interface (Fig. S28). This interpretation is consistent with the more negative zeta potential of E30Y28 in SIF compared with longer tyrosine-containing analogues, suggesting greater interfacial presentation of glutamate carboxylates under these conditions (Fig. 3B). Therefore, E30Y28 was selected as a model for evaluating pH-dependent changes in surface charge during sequential acidification (Fig. S29). The experiment demonstrates that the surface charge of E30Y28 becomes progressively less negative when acid is added to solution, indicating the protonation of negatively charged glutamic acid side chains.

Kinetics were studied to verify the timescale on which equilibrium drug adsorption was achieved, and whether it differed based on drug and pH. For gastrointestinal drug adsorption, the specific kinetic model or mechanistic regime that best fits early uptake is not highly clinically meaningful; what is instead important is whether the characteristic timescale of adsorption is fast relative to the timescales of gastric and intestinal transit. Since E30Y129 achieved high drug adsorption within relevant windows for overdose management, further rate law modeling was not pursued.

Adsorption capacity

Capacity studies were performed to determine whether larger tyrosine chain lengths increased drug adsorption. These studies followed the same method as adsorption kinetics experiments, except that the EYs were incubated with each of the drugs for 120 minutes, to ensure complete saturation. Further, while the 10 : 1 adsorbent-to-adsorbate mass ratio used in adsorption kinetics experiments demonstrated high uptake, a 13 : 1 adsorbent-to-adsorbate mass ratio was chosen for capacity experiments to push drug removal closer to 100%. The 13 : 1 adsorbent-to-adsorbate mass ratio was selected based on preliminary screening showing that the 10 : 1 condition produced high but incomplete removal for some adsorbate-adsorbent combinations. The higher ratio was therefore used to determine whether modestly increasing the adsorbent dose would achieve complete adsorption, while the 10 : 1 condition was used for kinetics to compare uptake rates under benchmark loading conditions. From a clinical standpoint, this meager increase in adsorbent-to-adsorbate mass ratio is still practical for an adsorbent dose, where reports suggest adsorbent doses between 10 to 40 times the amount of drug.[52] Full experimental methods are detailed in the SI.

The data demonstrate that the amount of adsorbed drug increases with larger tyrosine chain lengths (Fig. 4). In SGF, adsorption increased significantly from E30Y28 to E30Y79 for all four drugs (Fig. 4B). Further increases at longer tyrosine block lengths were significant for AMI and HCQ, whereas BUP and STR adsorption did not differ significantly among E30Y79, E30Y101, and E30Y129. This suggests that increasing tyrosine block length has the largest effect between E30Y28 and E30Y79, followed by a plateau at higher tyrosine contents. In SIF, AMI and STR adsorption increased significantly from E30Y79 to E30Y101 and E30Y129, while E30Y101 and E30Y129 were not significantly different from each other (Fig. 4C). For BUP, E30Y129 showed significantly greater adsorption than E30Y79 and E30Y101, whereas E30Y79 and E30Y101 were not significantly different. HCQ adsorption was high across all three polymers and did not differ significantly with tyrosine block length. Overall, these trends indicate that increasing the tyrosine block length enhances drug adsorption, likely by increasing the aromatic/hydrophobic domain available for drug-polymer interactions, although the benefit becomes less pronounced with larger tyrosine block lengths.

The trend in adsorption with longer tyrosine block lengths is less pronounced in SGF compared to SIF (Fig. 4). This likely reflects variations in particle size induced by the different pHs of the two media. In SIF (pH 6.8), deprotonation of glutamate side chains increases polymer hydrophilicity and promotes solvation of the polypeptide backbone, improving wettability and dispersibility in aqueous media. These effects favor the formation of smaller, better-dispersed assemblies with greater accessible surface area for drug adsorption (Fig. S15–S18).[53–55] In contrast, in SGF (pH 1.2), protonation of glutamate reduces charge repulsion and polymer hydration, encouraging hydrophobic collapse and the formation of larger aggregates (Fig. S15–S18). Aggregation under acidic conditions can sequester aromatic residues within the particle interior, thereby reducing the surface area available for drug binding.[53–55] This pH-responsive behavior is supported by the aforementioned control experiment with E30Y28 performed by acidification of SIF (Fig. S29).

Data for adsorption to E30Y28 are not compared to the rest of the EY series in SIF (Fig. 4C). As previously mentioned, E30Y28 featured few insoluble particles when viewed using transmitted light microscopy in SIF (Fig. 3C, 10× and 20×). Upon dispersion at 1 mg mL^{-1} in pH 8 deionized water, the sample appeared cloudy but translucent with no visible sedimentation (Fig. S28), which is visually consistent with colloidal assembly formation.[56] Particle size distribution data provides more evidence for the presence of colloidal assemblies in SIF, as it is the only polypeptide in the series that features a population of particles less than 100 nm in size (Fig. S12, blue, <100 nm).[57,58] As such, adsorption to E30Y28 in SIF was performed (Fig. S30), but is not directly compared to E30Y79, E30Y101, and E30Y129 in SIF since these polypeptides do not behave the same way, according to microscopy and particle size data (Fig. 3C, 10× and 20×; Fig. S12–S15). Furthermore, control studies indicate that the centrifugal filters used for the adsorption experiments do not adequately remove these <100 nm assemblies from solution, based on the elevated absorption of SIF filtrate after incubation with E30Y28 (Fig. S31). As such,

adsorption of AMI to E30Y28 in SIF cannot be interpreted using UV-Vis techniques since the high absorbance of the polypeptide blank in SIF interferes with accurate analysis (Fig. S32).

These capacity results demonstrate that EYs can achieve high and, in several cases, complete adsorption at clinically practical adsorbent-to-adsorbate mass ratios. The increase in adsorption with tyrosine block length demonstrates that performance can be optimized through controlled polymer design. Notably, the strong uptake observed across structurally and chemically distinct drugs that are commonly encountered in overdose scenarios demonstrates the relevance of this platform for gastrointestinal decontamination. Although complete drug adsorption is still not observed in SGF at a 13 : 1 ratio, extrapolation of the trend predicts complete adsorption at adsorbent-to-drug ratios below 40 : 1, which falls within established activated charcoal dosing guidelines for overdose treatment.[52] These features position EY polypeptides as a promising framework that can be further optimized for drug adsorption applications.

Isotherm modeling

Adsorption capacity experiments showed that E30Y129 exhibited the highest drug uptake at a 13 : 1 adsorbent-to-adsorbate mass ratio. As the top-performing formulation, E30Y129 was selected for subsequent studies to evaluate its adsorption profile *via* isotherm modeling. In these studies, separate samples with increasing amounts of polypeptide were incubated with a fixed drug concentration at 37 °C for 120 minutes. Following incubation, polypeptides were centrifuged using filter units (MWCO 3 kDa) to remove dissolved complexes and insoluble particles from the supernatant. Then, the supernatant was analyzed using UV-Vis to determine the concentration of remaining drug in solution (Fig. S16–S23). The data were then fit to the Langmuir isotherm to derive physical constants that quantify adsorbent characteristics, including maximum adsorption capacity (Q_{max}) and binding affinity (K_L). Full experimental details can be found in the SI.

Nonlinear adsorption isotherms were obtained for each drug in SGF and SIF using E30Y129 (Fig. S33A–S40A). At low equilibrium concentrations (C_e), the equilibrium adsorption capacity (Q_e) increased gradually, consistent with adsorption to accessible high-affinity sites on or within the polypeptide aggregates.[59] At higher C_e, several isotherms displayed steep increases in Q_e, reaching values approaching 1 g of drug adsorbed per g of polypeptide. This high-concentration behavior indicates adsorption beyond an ideal monolayer and likely reflects non-ideal uptake processes, including multilayer adsorption, drug–drug association within the adsorbed phase, or partitioning into hydrophobic aggregate domains.[60,61] Therefore, fitting to a Langmuir isotherm was only performed for low C_e, where uptake was most consistent with initial site-limited adsorption, to provide comparative apparent adsorption parameters across adsorbates and media (Fig. S33B–S40B). Accordingly, the reported maximum adsorption capacity (Q_{max}) values should be interpreted as apparent low-concentration monolayer capacities rather than absolute saturation capacities for the full adsorption process, and binding affinity (K_L) should be interpreted as an apparent affinity parameter for the initial adsorption regime. Although alternative isotherm models, including Hill-type cooperative adsorption models, can describe cooperative or multilayer adsorption processes,[62] application of these models using our experimental design required high-C_e adsorption measurements that would have necessitated material scales beyond the practical scope of this study.

Site availability and favorable interactions govern adsorption under the Langmuir isotherm model. When fit to this model, the data reveal that these factors contribute differently to overall adsorption depending on pH and the structural features of the drugs (Fig. 5). In SGF, AMI exhibits the highest Q_{max}, consistent with its large, hydrophobic aromatic network that may favor π-stacking interactions with E30Y129. In SIF, adsorption capacities increase due to a greater number of available binding sites when E30Y129 is deprotonated and more hydrated. This increase is least pronounced for adsorption of BUP, which features a sterically hindered cation that may limit interactions with glutamate residues.

Binding affinity trends further clarify the drug features that lead to higher interactions with E30Y129 (Fig. 5). In SGF, K_L values were within the same order of magnitude across the drug set. However, in SIF, these values were generally higher, with AMI and HCQ exhibiting the most favorable interactions. In SIF, the glutamate block can electrostatically bind cationic drugs, while the tyrosine block provides aromatic and hydrophobic surfaces for adsorption. Drugs like AMI and HCQ, which have larger aromatic networks and conformationally flexible aliphatic cations, may access a broader range of binding geometries, leading to stronger binding affinities. Both STR and BUP have smaller aromatic networks than AMI and HCQ. Further, the rigid structure of STR restricts accessibility of the aromatic ring and cation, whereas the cation is sterically hindered by the methyl group in BUP.

Since the Langmuir model was applied only to the initial low-C_e regime, the resulting parameters were used for comparative analysis rather than as complete descriptions of the full adsorption process. To further contextualize these values, the apparent capacities of E30Y129 were compared with reported adsorption capacities for other proposed oral detoxifying materials. These comparisons are not direct one-to-one evaluations because adsorption capacity depends on adsorbate structure, medium composition, concentration range, adsorbent loading, and model selection.[62,63] However, they provide a useful benchmark for evaluating the performance of EY polypeptides relative to other non-charcoal adsorbent platforms.

In simulated gastric (pH 1.2) and intestinal (pH 6.8) conditions, E30Y129 exhibited maximum adsorption capacity values ranging from 40 to 238 mg g^{-1} and binding affinities between 0.008 to 0.214 L g^{-1} (Fig. 5). These values fall within the ranges reported for adsorbent biopolymers in literature.[64–66] Further, E30Y129 also falls within the same order of magnitude as inorganic nanomaterial adsorbents including metal–organic

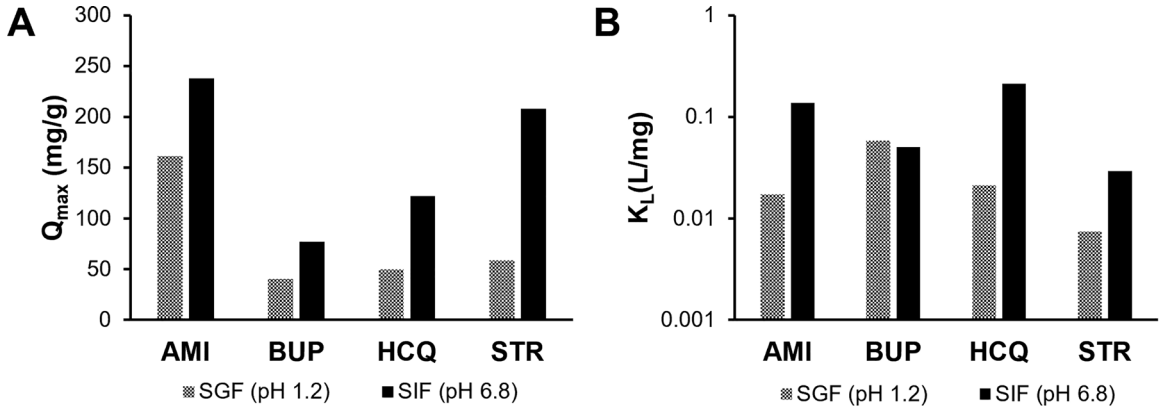

Q_{max}	SGF (pH 1.2)	SIF (pH 6.8)
AMI	161.3	238.1
BUP	40.5	77.5
HCQ	50.0	122.0
STR	58.8	208.3

K_L	SGF (pH 1.2)	SIF (pH 6.8)
AMI	0.0172	0.1386
BUP	0.0583	0.0505
HCQ	0.0210	0.2141
STR	0.0075	0.0294

Fig. 5 Apparent Langmuir adsorption parameters for E30Y129 adsorption in simulated gastrointestinal media. (A) Gives apparent maximum adsorption capacity (Q_{max}) values for amitriptyline (AMI), bupropion (BUP), hydroxychloroquine (HCQ), and strychnine (STR) adsorption to E30Y129 in simulated gastric fluid (SGF, pH 1.2) and simulated intestinal fluid (SIF, pH 6.8). (B) Shows apparent binding affinity (K_L) values for the same drug and medium conditions. Values were obtained by fitting the low equilibrium concentration (C_e) region of the adsorption isotherms to the linearized Langmuir model and are reported as apparent comparative parameters rather than absolute saturation capacities or global binding constants for the full adsorption process. Non-ideal adsorption behavior observed at higher C_e values is not captured by these fitted parameters. Tables below each plot provide the corresponding fitted values plotted in the bar charts.

frameworks that adsorb salicylates[67] and titanate nanotubes that adsorb paracetamol.[68]

The performance of E30Y129 is also competitive with AC for the adsorption of drugs with certain chemical characteristics. The maximum adsorption capacities for each drug with E30Y129 is within the same order of magnitude as those observed with AC (Table S1). In SGF, the adsorption capacity of E30Y129 for AMI was comparable to the value measured with AC, while in SIF the adsorption capacity of E30Y129 for STR approached that of AC. With the exception of AMI, the binding affinities for each drug with E30Y129 were also within the same order of magnitude as those observed with AC (Table S2). Further, the binding affinity of E30Y129 with HCQ in SIF approached that of AC. Since the reported E30Y129 adsorption capacity here represents the monolayer capacity as determined by Langmuir isotherm fitting, it is worth emphasizing that these values underestimate contributions from multilayer adsorption. However, these results demonstrate that polypeptide adsorbents can compete with AC in certain contexts, and merit further study for optimization in the context of high-capacity adsorption.

Since the goal of this proof-of-concept study was to determine whether E30Y129 could achieve meaningful adsorption of clinically relevant drugs, desorption from E30Y129 was not evaluated. However, these experiments are an important next step and will be pursued in future work to evaluate the robustness of E30Y129 as an adsorbent. Here, establishing adsorption performance and defining initial binding parameters serve as the foundation for such future studies.

Fed-state drug adsorption

The simulated biological media used in this study only contain salts and therefore model fasted-state gastrointestinal conditions. In contrast, fed-state conditions involve nutrient-rich food matrices that can alter the physicochemical environment and potentially influence drug-adsorbent interactions. Although a full investigation of fed-state effects across all drugs and polypeptides was beyond the scope of this work, we performed exploratory adsorption experiments for a subset of drugs with E30Y129 in the presence of a complex food matrix. These experiments were designed to provide initial insight into how nutrient-rich conditions may influence adsorption relative to fasted-state environments.

E30Y129 was selected because it was the best-performing polypeptide in this work and its adsorption behavior is well characterized through isotherm modeling. STR and HCQ were chosen for fed-state experiments because they bracket the structural and chemical diversity of the drug panel; STR represents a bulky, rigid polycyclic cation and HCQ is a more flexible polycationic molecule. Although their adsorption capacities on E30Y129 are comparable across SGF and SIF, their binding affinities differ substantially between these media (Fig. 5A and B). Studying these two drugs in the presence of food therefore allows us to observe whether fed-state conditions

disproportionately affect adsorption for molecules with similar capacities but distinct affinity profiles.

Adsorption under fed-state conditions was evaluated using a similar experimental design as the previous "starved" adsorption capacity studies. Briefly, a suspension of E30Y129 was prepared by dispersing the powder in either SGF or SIF. Next, solutions of STR and HCQ were prepared by dissolving the adsorbates in liquid baby formula calibrated to pH 1.2 or pH 6.8. Volumes of E30Y129 in simulated biological media were combined with the adsorbates in formula at the appropriate pH to achieve a 13 : 1 adsorbent-to-adsorbate mass ratio. By adding adsorbent dispersed in liquid to drug dissolved in formula, the experiment is designed to mimic the administration of an adsorbent for overdose treatment to remove drug in a non-fasted state. Matched control samples were prepared to account for matrix contributions to the signal, including drug-containing formula without adsorbent and blanks containing adsorbent and formula without drug. For HCQ, the presence of formula in solution did not greatly impact the amount of drug that was adsorbed in SIF and even increased the amount of drug adsorbed in SGF compared to the study in the absence of formula (Fig. 6). However, for STR, the presence of formula in solution led to a reduction in drug adsorption in both SGF and SIF. HCQ is likely adsorbed well in the presence of formula because adsorption to E30Y129 is more favorable than for STR (Fig. 5A and B). The Langmuir binding constants show that HCQ has higher affinity for E30Y129 in both SGF and SIF; binding affinity values for HCQ are 0.0210 in SGF and 0.2141 in SIF, whereas strychnine has binding affinity values of only 0.0075 in SGF and 0.0294 in SIF. Even though the maximum adsorption capacities of the drugs are comparable, interactions between HCQ and E30Y129 are more favorable.

When formula is added, components such as lipids, proteins, and other organic matter may partially block the polymer surface, compete for adsorption sites, or provide alternative environments for the drug in solution. These effects are expected to disproportionately impact adsorbates with weaker binding affinities. Since adsorption of STR to E30Y129 is less favorable, competition from the formula matrix may explain the reduction in STR adsorption (Fig. 6). In contrast, HCQ adsorption was largely retained in the presence of formula, suggesting that these interactions may be less sensitive to matrix competition under these conditions, potentially because of its higher apparent binding affinity. Thus, the effect of the

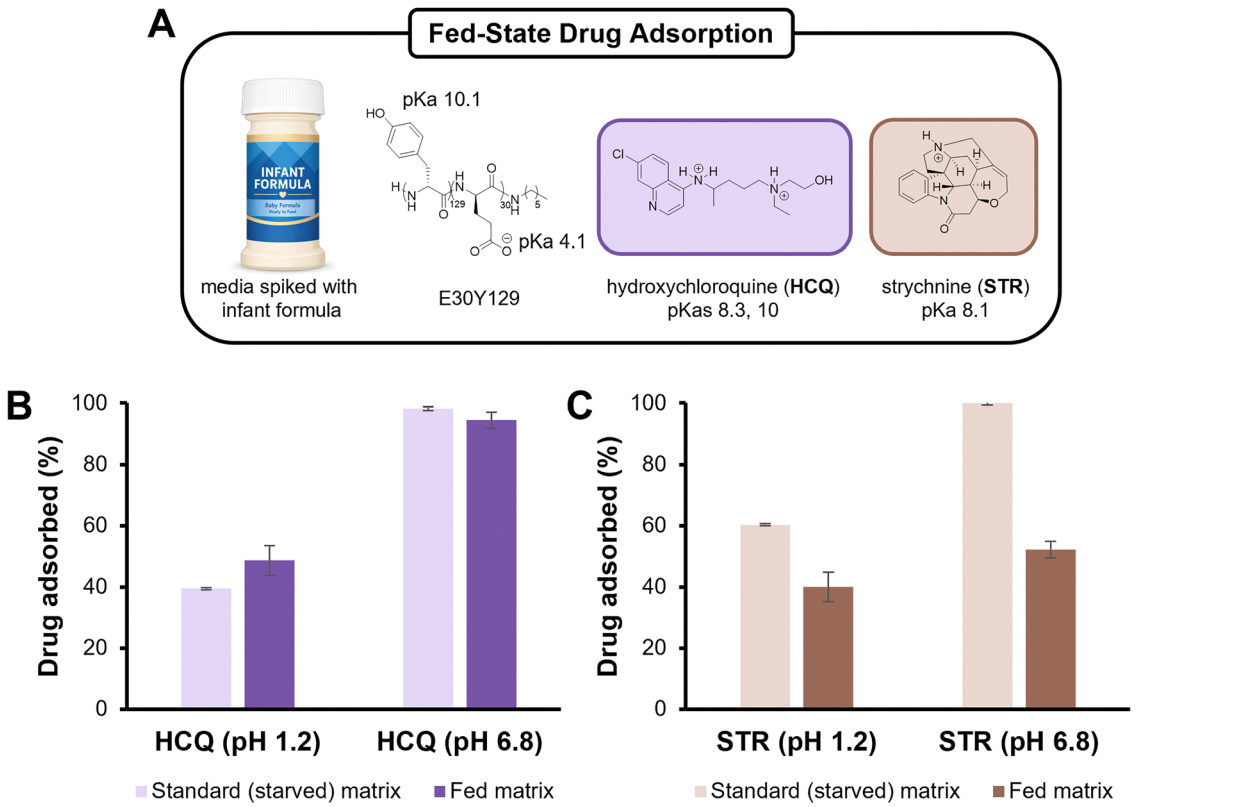

Fig. 6 Fed-state adsorption of hydroxychloroquine and strychnine to E30Y129. (A) shows the experimental design for evaluating drug adsorption in media containing infant formula as a model fed matrix, using E30Y129 as the adsorbent and hydroxychloroquine (HCQ) and strychnine (STR) as representative adsorbates. (B) shows HCQ adsorption to E30Y129 in standard simulated gastrointestinal media and the fed matrix at pH 1.2 and pH 6.8. (C) shows STR adsorption to E30Y129 in standard simulated gastrointestinal media and the fed matrix at pH 1.2 and pH 6.8. Adsorption experiments were performed at 37 °C using a 13 : 1 adsorbent-to-adsorbate mass ratio. Data are shown as mean ± standard deviation from triplicate measurements. Fed matrix experiments are interpreted as a preliminary *in vitro* assessment of matrix effects and are not intended to fully reproduce fed-state gastrointestinal conditions.

fed-state matrix was adsorbate-dependent, which is clinically relevant because oral adsorbents may be administered under variable gastrointestinal conditions. While background contributions from the formula matrix were accounted for using blank controls, the matrix may still alter drug behavior in solution or access to adsorption sites in ways that influence apparent adsorption. Therefore, these results should be interpreted as a preliminary *in vitro* investigation of matrix effects on adsorption to E30Y129 rather than direct evidence of *in vivo* fed-state performance.

Enzyme degradation

Digestive enzymes were intentionally omitted from the simulated gastric and intestinal fluids used for adsorption studies to isolate the effects of pH and drug chemistry on adsorption. Gastrointestinal enzymes were not expected to be primary drivers of drug binding, and their inclusion would have complicated interpretation of the molecular interactions responsible for adsorption to the polypeptides. However, because EYs contain peptide backbones that may undergo hydrolytic or enzymatic cleavage, an *in vitro* enzyme degradation study was performed as an initial assessment of proteolytic susceptibility under simplified gastrointestinal enzyme conditions.

E30Y28 was selected for enzyme degradation studies because it contains the shortest hydrophobic tyrosine block and exhibited the greatest apparent hydration in simulated gastrointestinal media. This provided a conservative condition for evaluating enzymatic susceptibility, as increased hydration was expected to promote greater interaction with digestive enzymes compared with more hydrophobic, tyrosine-rich analogues that remain less hydrated in solution.[69] Samples were incubated at 37 °C in simulated gastric fluid containing pepsin for 72 h and simulated intestinal fluid containing trypsin and α-chymotrypsin for 72 h. These incubation periods exceed typical physiological gastric and small-intestinal transit times and were selected as extended *in vitro* exposure conditions to assess whether gastrointestinal enzymes produce appreciable degradation of the bulk material, rather than to directly replicate *in vivo* residence times.[70]

Degradation was assessed using peptide backbone signals, which are shared by both glutamic acid and tyrosine repeat units and therefore provide a compositionally representative measure of bulk polypeptide integrity. After 72 h in SGF containing pepsin, E30Y28 exhibited modest degradation, with the number-average repeat units decreasing from 58 to 55 (Fig. S41). Under acidic conditions, reduced polymer hydration is expected to limit solvent penetration and enzyme accessibility, resulting in slower degradation.[69] In contrast, exposure to trypsin and α-chymotrypsin in SIF led to a larger reduction in number-average repeat units, decreasing from 58 to 47 (Fig. S42). This enhanced degradation is consistent with increased polymer hydration under intestinal conditions, which may facilitate improved enzyme access to the peptide backbone.

These results indicate that E30Y28 remains largely intact under the tested extended enzyme exposures but is susceptible to gradual degradation, particularly under intestinal protease conditions. However, this assay should be interpreted as a preliminary *in vitro* assessment of proteolytic susceptibility rather than a complete model of gastrointestinal degradation or *in vivo* residence time. The media used here include representative digestive enzymes but do not capture the full complexity of the gastrointestinal tract, including additional enzymes, bile salts, food components, motility, microbiota, or clearance. In addition, ^{1}H NMR reports changes in bulk polymer composition and number-average repeat unit estimates, but it is not sensitive to subtle chain scission events that do not substantially alter the integral values. Molecular weight analysis by GPC could not be reliably performed for these deprotected polypeptides because of incompatibility of deprotected polypeptides with available instrument conditions. Future studies using gel electrophoresis, matrix-assisted laser desorption/ionization time-of-flight mass spectrometry, assays for newly formed primary amines, *ex vivo* models, or *in vivo* analysis would be needed to resolve degradation pathways and evaluate gastointestinal residence, clearance, accumulation, or obstruction risk under physiological conditions.

Cell viability

Having evaluated preliminary enzymatic susceptibility under simulated gastrointestinal conditions, we next examined mammalian cell interactions to assess the initial cytocompatibility of the EY polypeptides. Polypeptides are generally attractive for biomedical applications because of their structural and chemical similarity to endogenous biomolecules. However, hydrophobic domains within polypeptide materials can contribute to cytotoxic effects, particularly at high concentrations or when hydrophobic segments are solvent-exposed.[71,72] Therefore, E30Y129 was selected as a representative model for cytocompatibility screening because it contains the longest hydrophobic tyrosine block of the EY series.

The viability of RAW 264.7 murine macrophages and NIH 3T3 fibroblasts was evaluated after exposure to E30Y129 over a concentration range of 1–250 μg mL^{-1}. These cell lines were selected as initial screening models because fibroblasts and macrophages are commonly used to evaluate tissue-facing and immune cell responses to biomaterials.[73] Fibroblasts are involved in extracellular matrix production, wound healing, and tissue remodeling,[74] whereas macrophages play central roles in immune surveillance, inflammation, and foreign body responses.[75] However, these cell lines are not direct models of the gastrointestinal epithelium, and therefore these experiments should be interpreted as an initial cytocompatibility assessment rather than a complete evaluation of gastrointestinal cellular compatibility.

NIH 3T3 cell viabilities were comparable to untreated controls following exposure to E30Y129 (Fig. 7A and B). Although mean cell viabilities were slightly higher than the control at intermediate concentrations, these differences were not statistically significant (p = 0.11). Single-factor analysis of variance (ANOVA) indicated no dose-dependent decrease in NIH 3T3 viability, supporting the absence of overt cytotoxic effects within the tested concentration range.

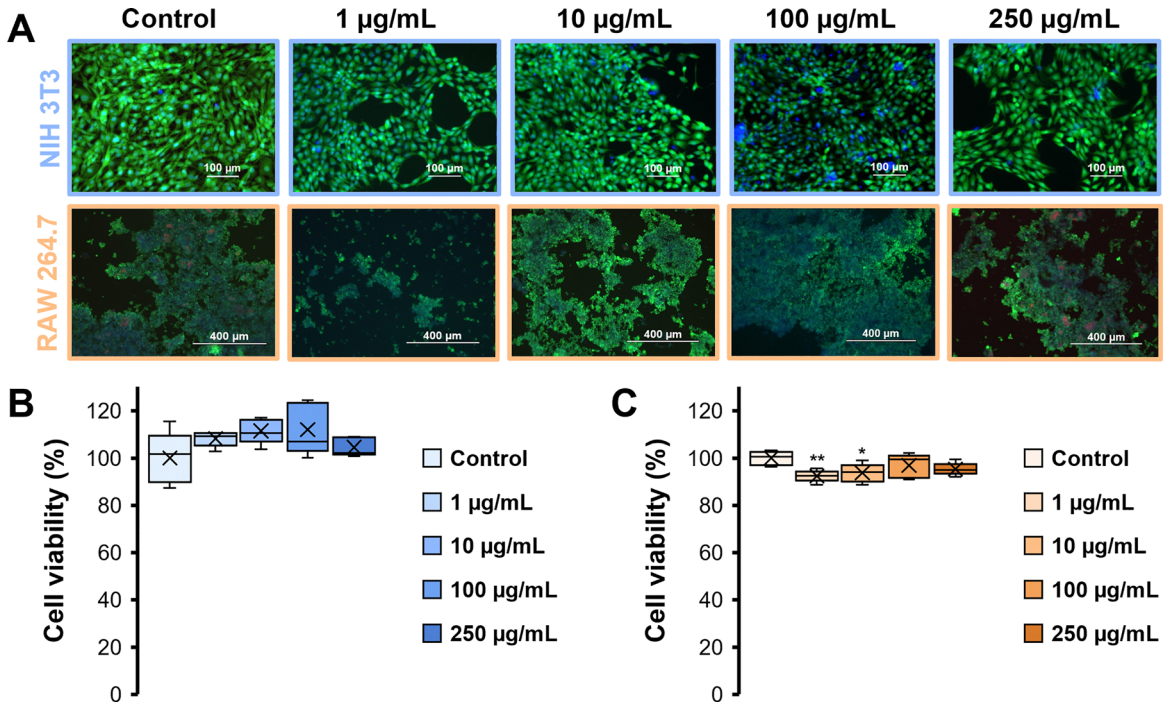

Fig. 7 Cytocompatibility of E30Y129 with NIH 3T3 fibroblasts and RAW 264.7 macrophages. (A) Shows representative fluorescence microscopy images of NIH 3T3 fibroblasts (top row) and RAW 264.7 macrophages (bottom row) following 48 h exposure to E30Y129 at concentrations ranging from 1 to 250 μg mL^{-1}, compared to untreated controls. Cells were stained with Hoechst 33342 to visualize nuclei and Calcein acetoxymethyl ester (AM) to identify viable cells. (B) Shows NIH 3T3 fibroblast viability compared to untreated controls. (C) Shows RAW 264.7 macrophage viability compared to untreated controls. Data are shown as mean ± standard deviation from five independent fluorescence measurements per condition. Scale bars are 100 μm for NIH 3T3 fibroblasts and 400 μm for RAW 264.7 macrophages. Statistical significance was determined by one way analysis of variance (ANOVA) followed by Dunnett's *post hoc* test relative to untreated controls. Significance is denoted as * = $p < 0.05$, ** = $p < 0.01$, *** = $p < 0.001$, and ns = not significant. No dose dependent decrease in viability was observed for either cell type across the tested concentration range.

RAW 264.7 macrophage viabilities were generally high following exposure to E30Y129 across the tested concentration range (Fig. 7A and C). One-way ANOVA indicated a statistically significant effect of concentration on viability ($p = 0.025$). *Post hoc* analysis using Dunnett's test showed modest but statistically significant decreases in viability at 1 μg mL^{-1} and 10 μg mL^{-1} relative to the untreated control, whereas no significant decrease was observed at the higher concentrations of 100 or 250 μg mL^{-1}. Because the reduction in viability was small in magnitude and did not increase with concentration, these results do not indicate a dose-dependent cytotoxic response. Instead, the RAW 264.7 data suggest minor, nonmonotonic changes in macrophage viability under the tested conditions, with no overt cytotoxicity observed at the highest E30Y129 concentrations.

Fluorescence microscopy further supported preserved cell morphology following E30Y129 exposure. NIH 3T3 fibroblasts and RAW 264.7 macrophages retained visible nuclei and actin cytoskeletal staining after treatment, consistent with maintained cell attachment and morphology (Fig. 7A). At higher polypeptide concentrations, non-cellular fluorescent regions were observed in both fibroblast and macrophage cultures and were attributed to E30Y129 aggregates. Depending on the imaging channel, these aggregates appeared more intensely in the Hoechst channel or more faintly in the propidium iodide channel. Bright-field imaging confirmed that these features corresponded to material aggregates rather than nuclei or dead cells. Because aggregates can potentially interfere with fluorescence-based viability measurements through light scattering, physical occlusion, or nonspecific fluorescence, viability was assessed using direct fluorescence imaging combined with MATLAB-based cell counting rather than bulk plate fluorescence alone. This image-based approach allowed cellular nuclei to be distinguished from non-cellular aggregate features based on morphology, size, channel overlap, and bright-field correspondence, minimizing the likelihood that material aggregates were counted as viable or nonviable cells. Overall, E30Y129 did not induce overt cytotoxicity toward NIH 3T3 fibroblasts or RAW 264.7 macrophages under the tested conditions, although future studies using gastrointestinally relevant cell models such as Caco-2 or HT-29 cells will be needed to evaluate epithelial compatibility more directly.[76,77]

Conclusion

This work establishes poly(glutamic acid-*block*-tyrosine) peptides (EYs) as a tunable platform for gastrointestinal drug adsorption. These materials exhibit improved adsorption of basic drugs relative to previously reported KEY polypeptide

adsorbents and provide a framework for designing adsorbents with controllable composition, aggregation behavior, and drug-binding properties.[25] By systematically varying tyrosine block length while maintaining a fixed-length E30 glutamic acid block, this study demonstrates that adsorption behavior can be modulated through amino acid composition and block length.

Across a drug panel consisting of amitriptyline (AMI), bupropion (BUP), hydroxychloroquine (HCQ), and strychnine (STR), EYs demonstrated measurable adsorption under simulated gastric and intestinal conditions. Adsorption was pH-dependent, with enhanced adsorption generally observed under intestinal conditions where deprotonated glutamate residues can contribute to electrostatic interactions. Increasing tyrosine content generally improved adsorption performance, although the relationship between tyrosine block length and adsorption was not strictly monotonic for all adsorbates. This behavior indicates that adsorption is governed by a combination of electrostatic, aromatic, hydrophobic, and aggregate-dependent effects rather than tyrosine content alone. The highest-performing formulation, E30Y129, exhibited apparent maximum adsorption capacities and binding affinities that were competitive with reported biopolymer adsorbents, other proposed oral detoxifying nanomaterials, and activated charcoal for select drugs.

Langmuir-derived parameters provided useful comparative descriptors of E30Y129 adsorption in the low-concentration (C_e) regime, while the full isotherm profiles indicated non-ideal adsorption behavior at higher drug concentrations. Therefore, the reported maximum adsorption capacity (Q_{max}) and binding affinity (K_L) values should be interpreted as apparent adsorption parameters, as high C_e data was not modelled and is therefore not accounted for in these values. The adsorption trends, together with structure–property analysis, provide design criteria for future polypeptide adsorbents by identifying drug features and material properties that promote favorable uptake. Fed-state experiments further showed that matrix effects were adsorbate-dependent, with food components reducing STR adsorption while HCQ adsorption appeared largely consistent under the tested conditions. This finding highlights the need to evaluate gastrointestinal adsorbents on a drug-specific basis under increasingly complex media conditions.

Beyond adsorption performance, EYs displayed properties relevant to future translational development, while also identifying important limitations that require further study. Preliminary *in vitro* enzyme degradation experiments indicated that E30Y28 remained partially intact under extended simulated gastrointestinal enzyme exposure but was susceptible to gradual degradation, particularly under intestinal protease conditions. These results should be interpreted as an initial assessment of proteolytic susceptibility rather than evidence of *in vivo* gastrointestinal stability, residence time, clearance, accumulation behavior, or obstruction risk. Cytocompatibility studies showed that E30Y129 was well tolerated by NIH 3T3 fibroblasts and did not produce dose-dependent cytotoxicity in RAW 264.7 macrophages under the tested conditions, although these cell lines are not direct models of the gastrointestinal epithelium.

Taken together, this proof-of-concept study demonstrates that synthetic polypeptides can be engineered as drug adsorbents with tunable adsorption behavior, preliminary cytocompatibility, and enzymatically degradable peptide backbones. Future work should evaluate drug desorption and retention during gastrointestinal transit, adsorption performance in more complex fed-state and bile-containing media, compatibility with gastrointestinal epithelial models, formulation behavior, and *in vivo* efficacy and safety. These studies will be necessary to define the therapeutic potential of polypeptide adsorbents as enterosorbents for overdose treatment.

Author contributions

Hunter Wood: conceptualization, methodology, experimentation, data analysis, and writing. Joseph Dosch: experimentation and data analysis. Stella Trickett: experimentation and data analysis. Juhi Singh: experimentation and data analysis. Farin M. Weinger: experimentation and data analysis. Gerald J. Wang: data analysis. Dazhe Cao: conceptualization, methodology, and data analysis. Stefanie Sydlik: conceptualization, methodology, writing, supervision, and resources.

Conflicts of interest

The authors declare no competing interests.

Data availability

The data supporting this study are included within the supplementary information (SI). Supplementary information: includes a complete list of materials; characterization methods; synthetic and experimental methods; ^{1}H NMR characterization of monomers, the macroinitiator, and protected and deprotected polymers (Fig. S1–S11); particle size characterization of polymers in simulated gastric fluid (SGF) and simulated intestinal fluid (SIF) (Fig. S12–S15); UV-Vis calibration curves (Fig. S16–S23); adsorption kinetics in SGF and SIF (Fig. S24–S27); E30Y28 colloidal behavior, zeta potential acidification, apparent SIF adsorption data, and filtration controls (Fig. S28–S32); adsorption isotherm analyses and linearized Langmuir fits in SGF and SIF (Fig. S33–S40); comparison tables of apparent maximum adsorption capacities and apparent binding affinities for E30Y129 and activated charcoal (Tables S1 and S2); and ^{1}H NMR characterization of polypeptides after prolonged exposure to gastrointestinal enzymes to assess bulk material degradation (Fig. S41 and S42). See DOI: https://doi.org/10.1039/d6tb00121a.

References

1 S. Fujita-Imazu, J. Xie, B. Dhungel, X. Wang, Y. Wang, P. Nguyen, J. Khin Maung Soe, J. Li and S. Gilmour, Evolving Trends in Drug Overdose Mortality in the USA from 2000 to

2020: An Age-Period-Cohort Analysis, *eClinicalMedicine*, 2023, **61**, 102079, DOI: 10.1016/j.eclinm.2023.102079.
2 Y. Zhao, Y. Liu, F. Lv, X. He, W. H. Ng, S. Qiu, L. Zhang, Z. Xing, Y. Guo, J. Zu, Y. H. Yeo and F. Ji, Temporal Trend of Drug Overdose-Related Deaths and Excess Deaths during the COVID-19 Pandemic: A Population-Based Study in the United States from 2012 to 2022, *eClinicalMedicine*, 2024, **74**, 102752, DOI: 10.1016/j.eclinm.2024.102752.
3 L. C. G. Hoegberg, G. Shepherd, D. M. Wood, J. Johnson, R. S. Hoffman, E. M. Caravati, W. L. Chan, S. W. Smith, K. R. Olson and S. Gosselin, Systematic Review on the Use of Activated Charcoal for Gastrointestinal Decontamination Following Acute Oral Overdose, *Clin. Toxicol.*, 2021, **59**(12), 1196–1227, DOI: 10.1080/15563650.2021.1961144.
4 K. Skov, N. A. Graudal and G. Jürgens, The Effect of Activated Charcoal on Drug Exposure Following Intravenous Administration: A Meta-Analysis, *Basic Clin. Pharmacol. Toxicol.*, 2021, **128**(4), 568–578, DOI: 10.1111/bcpt.13553.
5 B. Zieliński, P. Miądlicki and J. Przepiórski, Development of Activated Carbon for Removal of Pesticides from Water: Case Study, *Sci. Rep.*, 2022, **12**, 20869, DOI: 10.1038/s41598-022-25247-6.
6 L. Roivas and P. J. Neuvonen, Drug Adsorption onto Activated Charcoal as a Means of Formulation, *Methods Find. Exp. Clin. Pharmacol.*, 1994, **16**(5), 367–372.
7 E. P. Krenzelok and M. B. Heller, Effectiveness of Commercially Available Aqueous Activated Charcoal Products, *Ann. Emerg. Med.*, 1987, **16**(12), 1340–1343, DOI: 10.1016/s0196-0644(87)80415-8.
8 A. J. Juhola and E. O. Wiig, Pore Structure in Activated Charcoal. I. Determination of Micro Pore Size Distribution, *J. Am. Chem. Soc.*, 1949, **71**(6), 2069–2077, DOI: 10.1021/ja01174a050.
9 G. M. Burke, D. E. Wurster, M. J. Berg, P. Veng-Pedersen and D. D. Schottelius, Surface Characterization of Activated Charcoal by X-Ray Photoelectron Spectroscopy (XPS): Correlation with Phenobarbital Adsorption Data, *Pharm. Res.*, 1992, **9**(1), 126–130, DOI: 10.1023/a:1018900431661.
10 H. A. Alhashimi and C. B. Aktas, Life Cycle Environmental and Economic Performance of Biochar Compared with Activated Carbon: A Meta-Analysis, *Resour., Conserv. Recycl.*, 2017, **118**, 13–26, DOI: 10.1016/j.resconrec.2016.11.016.
11 J. Silberman; M. A. Galuska and A. Taylor, Activated Charcoal, in *StatPearls*, StatPearls Publishing, Treasure Island (FL), 2025.
12 C. R. Harris and D. Filandrinos, Accidental Administration of Activated Charcoal into the Lung: Aspiration by Proxy, *Ann. Emerg. Med.*, 1993, **22**(9), 1470–1473, DOI: 10.1016/S0196-0644(05)81998-5.
13 D. G. Menzies, A. Busuttil and L. F. Prescott, Fatal Pulmonary Aspiration of Oral Activated Charcoal, *BMJ*, 1988, **297**(6646), 459–460, DOI: 10.1136/bmj.297.6646.459.
14 C. G. Elliott, T. V. Colby, T. M. Kelly and H. G. Hicks, Charcoal Lung. Bronchiolitis Obliterans after Aspiration of Activated Charcoal, *Chest*, 1989, **96**(3), 672–674, DOI: 10.1378/chest.96.3.672.
15 F. R. Justiniani, R. Hippalgaonkar and L. O. Martinez, Charcoal-Containing Empyema Complicating Treatment for Overdose, *Chest*, 1985, **87**(3), 404–405, DOI: 10.1378/chest.87.3.404.
16 K. B. Goulbourne and J. E. Cisek, Small-Bowel Obstruction Secondary to Activated Charcoal and Adhesions, *Ann. Emerg. Med.*, 1994, **24**(1), 108–110, DOI: 10.1016/s0196-0644(94)70170-9.
17 T. K. Aljohani, A. M. Alshamrani, A. M. Alzahrani and R. A. Sairafi, A Rare Case of Small Bowel Obstruction Secondary to Activated Charcoal Administration, *J. Surg. Case Rep.*, 2019, **2019**(2), rjz033, DOI: 10.1093/jscr/rjz033.
18 Y. Shen, X. Fu, W. Fu and Z. Li, Biodegradable Stimuli-Responsive Polypeptide Materials Prepared by Ring Opening Polymerization, *Chem. Soc. Rev.*, 2015, **44**(3), 612–622, DOI: 10.1039/C4CS00271G.
19 Z. Song, Z. Han, S. Lv, C. Chen, L. Chen, L. Yin and J. Cheng, Synthetic Polypeptides: From Polymer Design to Supramolecular Assembly and Biomedical Application, *Chem. Soc. Rev.*, 2017, **46**(21), 6570–6599, DOI: 10.1039/C7CS00460E.
20 X. Zhang, S. Fu, B. Zhao, Y. Liu, R. S. Seruya and F. Zhang, Polypeptide-Protein Conjugation: A New Paradigm for Therapeutic Protein Delivery, *J. Controlled Release*, 2025, **384**, 113953, DOI: 10.1016/j.jconrel.2025.113953.
21 T. J. Deming, Synthetic Polypeptides for Biomedical Applications, *Prog. Polym. Sci.*, 2007, **32**(8), 858–875, DOI: 10.1016/j.progpolymsci.2007.05.010.
22 M. Rabe, D. Verdes and S. Seeger, Understanding Protein Adsorption Phenomena at Solid Surfaces, *Adv. Colloid Interface Sci.*, 2011, **162**(1), 87–106, DOI: 10.1016/j.cis.2010.12.007.
23 Y. Yamamoto, W. Yih Heah and K. Tashiro, Functional Oligo- and Polypeptide Assemblies for Photochemical, Optical and Electronic Applications, *Mater. Horiz.*, 2024, **11**(14), 3203–3212, DOI: 10.1039/D4MH00218K.
24 H. Wood, S. Trickett, J. Dosch, F. Weinger, D. Flaherty and S. Sydlik, Tuning Adsorption and Morphology in Poly(Glutamic Acid) via Controlled Acidic Partial Deprotection, *Polym. Int.*, 2026, **75**(6), 490–497, DOI: 10.1002/pi.70070.
25 K. E. Eckhart, H. B. Wood, T. A. Taoufik, M. E. Wolf, D. J. Cao and S. A. Sydlik, Aromatic Polypeptide Amphiphiles for Drug Adsorption: A New Approach for Drug Overdose Treatment, *RSC Appl. Polym.*, 2024, **2**(1), 47–61, DOI: 10.1039/D3LP00082F.
26 S. Zhang, A Reliable and Efficient First Principles-Based Method for Predicting pKa Values. 4. Organic Bases, *J. Comput. Chem.*, 2012, **33**(31), 2469–2482, DOI: 10.1002/jcc.23068.
27 L. Gaohua, X. Miao and L. Dou, Crosstalk of Physiological pH and Chemical pKa under the Umbrella of Physiologically Based Pharmacokinetic Modeling of Drug Absorption, Distribution, Metabolism, Excretion, and Toxicity, *Expert Opin. Drug Metab. Toxicol.*, 2021, **17**(9), 1103–1124, DOI: 10.1080/17425255.2021.1951223.
28 W. R. Forsyth, J. M. Antosiewicz and A. D. Robertson, Empirical Relationships between Protein Structure and

Carboxyl pKa Values in Proteins, *Proteins*, 2002, **48**(2), 388–403, DOI: 10.1002/prot.10174.

29 J. Sun, X. Jiang, Y. Zhou, J. Fan and G. Zeng, Microfiltration Membranes for the Removal of Bisphenol A from Aqueous Solution: Adsorption Behavior and Mechanism, *Water*, 2022, **14**(15), 2306, DOI: 10.3390/w14152306.

30 J. Zou, J. Fan, X. He, S. Zhang, H. Wang and K. L. Wooley, A Facile Glovebox-Free Strategy to Significantly Accelerate the Syntheses of Well-Defined Polypeptides by N-Carboxyanhydride (NCA) Ring Opening Polymerizations, *Macromolecules*, 2013, **46**(10), 4223–4226, DOI: 10.1021/ma4007939.

31 M. S. Kim, K. Dayananda, E. K. Choi, H. J. Park, J. S. Kim and D. S. Lee, Synthesis and Characterization of Poly(l-Glutamic Acid)-*Block*-Poly(l-Phenylalanine), *Polymer*, 2009, **50**(10), 2252–2257, DOI: 10.1016/j.polymer.2009.03.015.

32 V. Dmitrovic, G. J. M. Habraken, M. M. R. M. Hendrix, W. J. E. M. Habraken, A. Heise, G. De With and N. A. J. M. Sommerdijk, Random Poly(Amino Acid)s Synthesized by Ring Opening Polymerization as Additives in the Biomimetic Mineralization of $CaCO_3$, *Polymers*, 2012, **4**(2), 1195–1210, DOI: 10.3390/polym4021195.

33 S. Stefanovic, K. McCormick, S. Fattah, R. Brannigan, S.-A. Cryan and A. Heise, Star-Shaped Poly(L-Lysine) with Polyester Bis-MPA Dendritic Core as Potential Degradable Nano Vectors for Gene Delivery, *Polym. Chem.*, 2023, **14**(27), 3151–3159, DOI: 10.1039/D3PY00346A.

34 D. J. da Silva, G. M. Cobe, R. C. Vlasman and L. H. Catalani, Self-Assembly of pH-Responsive Star-Shaped Amphiphilic Polypeptides Based on L-Lysine and L-Leucine, *ACS Polym. Au*, 2025, **5**(6), 907–918, DOI: 10.1021/acspolymersau.5c00098.

35 A. Barth, Infrared Spectroscopy of Proteins, *Biochim. Biophys. Acta, Bioenerg.*, 2007, **1767**(9), 1073–1101, DOI: 10.1016/j.bbabio.2007.06.004.

36 M. Wolpert and P. Hellwig, Infrared Spectra and Molar Absorption Coefficients of the 20 Alpha Amino Acids in Aqueous Solutions in the Spectral Range from 1800 to 500cm−1, *Spectrochim. Acta, Part A*, 2006, **64**(4), 987–1001, DOI: 10.1016/j.saa.2005.08.025.

37 J. Stetefeld, S. A. McKenna and T. R. Patel, Dynamic Light Scattering: A Practical Guide and Applications in Biomedical Sciences, *Biophys. Rev.*, 2016, **8**(4), 409–427, DOI: 10.1007/s12551-016-0218-6.

38 A. Hawe, W. L. Hulse, W. Jiskoot and R. T. Forbes, Taylor Dispersion Analysis Compared to Dynamic Light Scattering for the Size Analysis of Therapeutic Peptides and Proteins and Their Aggregates, *Pharm. Res.*, 2011, **28**(9), 2302–2310, DOI: 10.1007/s11095-011-0460-3.

39 C. Urban and P. Schurtenberger, Characterization of Turbid Colloidal Suspensions Using Light Scattering Techniques Combined with Cross-Correlation Methods, *J. Colloid Interface Sci.*, 1998, **207**(1), 150–158, DOI: 10.1006/jcis.1998.5769.

40 S. Fraden and G. Maret, Multiple Light Scattering from Concentrated, Interacting Suspensions, *Phys. Rev. Lett.*, 1990, **65**(4), 512–515, DOI: 10.1103/PhysRevLett.65.512.

41 A. Yu Dzhuzha, I. I. Tarasenko, L. I. Atanase, A. Lavrentieva and E. G. Korzhikova-Vlakh, Amphiphilic Polypeptides Obtained by the Post-Polymerization Modification of Poly(Glutamic Acid) and Their Evaluation as Delivery Systems for Hydrophobic Drugs, *Int. J. Mol. Sci.*, 2023, **24**(2), 1049, DOI: 10.3390/ijms24021049.

42 A. Della Porta, K. Bornstein, A. Coye, T. Montrief, B. Long and M. A. Parris, Acute Chloroquine and Hydroxychloroquine Toxicity: A Review for Emergency Clinicians, *Am. J. Emerg. Med.*, 2020, **38**(10), 2209–2217, DOI: 10.1016/j.ajem.2020.07.030.

43 A. A. Alberter; A. J. Chambers and B. K. Wills, Bupropion Toxicity, in *StatPearls*, StatPearls Publishing, Treasure Island (FL), 2025.

44 H. K. R. Thanacoody and S. H. L. Thomas, Tricyclic Antidepressant Poisoning: Cardiovascular Toxicity, *Toxicol. Rev.*, 2005, **24**(3), 205–214, DOI: 10.2165/00139709-200524030-00013.

45 D. M. Wood, E. Webster, D. Martinez, P. I. Dargan and A. L. Jones, Case Report: Survival after Deliberate Strychnine Self-Poisoning, with Toxicokinetic Data, *Crit. Care*, 2002, **6**(5), 456–459, DOI: 10.1186/cc1549.

46 G. Ersan, Y. Kaya, M. S. Ersan, O. G. Apul and T. Karanfil, Adsorption Kinetics and Aggregation for Three Classes of Carbonaceous Adsorbents in the Presence of Natural Organic Matter, *Chemosphere*, 2019, **229**, 515–524, DOI: 10.1016/j.chemosphere.2019.05.014.

47 J. Villaverde, W. van Beinum, S. Beulke and C. D. Brown, The Kinetics of Sorption by Retarded Diffusion into Soil Aggregate Pores, *Environ. Sci. Technol.*, 2009, **43**(21), 8227–8232, DOI: 10.1021/es9015052.

48 M. R. C. Marques, R. Loebenberg and M. Almukainzi, Simulated Biological Fluids with Possible Application in Dissolution Testing, *Dissolution Technol.*, 2011, **18**(3), 15–28, DOI: 10.14227/DT180311P15.

49 J.-H. Deng, J. Luo, Y.-L. Mao, S. Lai, Y.-N. Gong, D.-C. Zhong and T.-B. Lu, π–π Stacking Interactions: Non-Negligible Forces for Stabilizing Porous Supramolecular Frameworks, *Sci. Adv.*, 2020, **6**(2), eaax9976, DOI: 10.1126/sciadv.aax9976.

50 T. Basu, S. Das and S. Majumdar, Elucidating the Influence of Electrostatic Force on the Re-Arrangement of H-Bonds of Protein Polymers in the Presence of Salts, *Soft Matter*, 2024, **20**(10), 2361–2373, DOI: 10.1039/d3sm01440a.

51 G. Schreiber and A. R. Fersht, Rapid, Electrostatically Assisted Association of Proteins, *Nat. Struct. Biol.*, 1996, **3**(5), 427–431, DOI: 10.1038/nsb0596-427.

52 T. Zellner, D. Prasa, E. Färber, P. Hoffmann-Walbeck, D. Genser and F. Eyer, The Use of Activated Charcoal to Treat Intoxications, *Dtsch. Arztebl. Int.*, 2019, **116**(18), 311–317, DOI: 10.3238/arztebl.2019.0311.

53 P. Batys, M. Morga, P. Bonarek and M. Sammalkorpi, pH-Induced Changes in Polypeptide Conformation: Force-Field Comparison with Experimental Validation, *J. Phys. Chem. B*, 2020, **124**(14), 2961–2972, DOI: 10.1021/acs.jpcb.0c01475.

54 C. B. Stanley and H. H. Strey, Osmotically Induced Helix-Coil Transition in Poly(Glutamic Acid, *Biophys. J.*, 2008, **94**(11), 4427–4434, DOI: 10.1529/biophysj.107.122705.

55 M. Geoghegan, Weak Polyelectrolyte Brushes, *Soft Matter*, 2022, **18**(13), 2500–2511, DOI: 10.1039/D2SM00005A.

56 A. Manosroi, C. Chankhampan, H. Ofoghi, W. Manosroi and J. Manosroi, Low Cytotoxic Elastic Niosomes Loaded with Salmon Calcitonin on Human Skin Fibroblasts, *Hum. Exp. Toxicol.*, 2013, **32**(1), 31–44, DOI: 10.1177/0960327112454892.

57 O. Korovkina, D. Polyakov, V. Korzhikov-Vlakh and E. Korzhikova-Vlakh, Stimuli-Responsive Polypeptide Nanoparticles for Enhanced DNA Delivery, *Molecules*, 2022, **27**(23), 8495, DOI: 10.3390/molecules27238495.

58 J. A. MacKay, M. Chen, J. R. McDaniel, W. Liu, A. J. Simnick and A. Chilkoti, Self-Assembling Chimeric Polypeptide-Doxorubicin Conjugate Nanoparticles That Abolish Tumours after a Single Injection, *Nat. Mater.*, 2009, **8**(12), 993–999, DOI: 10.1038/nmat2569.

59 K. C. Ng, M. Burhan, M. W. Shahzad and A. B. Ismail, A Universal Isotherm Model to Capture Adsorption Uptake and Energy Distribution of Porous Heterogeneous Surface, *Sci. Rep.*, 2017, **7**(1), 10634, DOI: 10.1038/s41598-017-11156-6.

60 F. Wang, M. Zhang, W. Sha, Y. Wang, H. Hao, Y. Dou and Y. Li, Sorption Behavior and Mechanisms of Organic Contaminants to Nano and Microplastics, *Molecules*, 2020, **25**(8), 1827, DOI: 10.3390/molecules25081827.

61 S. Shimizu and N. Matubayasi, Understanding Sorption Mechanisms Directly from Isotherms, *Langmuir*, 2023, **39**(17), 6113–6125, DOI: 10.1021/acs.langmuir.3c00256.

62 N. Ayawei, A. N. Ebelegi and D. Wankasi, Modelling and Interpretation of Adsorption Isotherms, *J. Chem.*, 2017, **2017**(1), 3039817, DOI: 10.1155/2017/3039817.

63 H. Alkhaldi, S. Alharthi, S. Alharthi, A. H. AlGhamdi, M. Y. AlZahrani, A. S. Mahmoud, L. Galal Amin, N. Hamad Al-Shaalan, E. W. Boraie, S. M. Attia, S. Ali Al-Gahtany, N. Aldaleeli, M. M. Ghobashy, I. A. Sharshir, M. Madani, R. Darwesh and F. S. Abaza, Sustainable Polymeric Adsorbents for Adsorption-Based Water Remediation and Pathogen Deactivation: A Review, *RSC Adv.*, 2024, **14**(45), 33143–33190, DOI: 10.1039/D4RA05269B.

64 A. M. Skwierawska, D. Nowacka, P. Nowicka, S. Rosa and K. Kozłowska-Tylingo, Structural Adaptive, Self-Separating Material for Removing Ibuprofen from Waters and Sewage, *Materials*, 2021, **14**(24), 7697, DOI: 10.3390/ma14247697.

65 B. Sukhbaatar, B. Yoo and J.-H. Lim, Metal-Free High-Adsorption-Capacity Adsorbent Derived from Spent Coffee Grounds for Methylene Blue, *RSC Adv.*, 2021, **11**(9), 5118–5127, DOI: 10.1039/D0RA09550H.

66 N. Ullah, Z. Ali, A. S. Khan, B. Adalat, A. Nasrullah and S. B. Khan, Preparation and Dye Adsorption Properties of Activated Carbon/Clay/Sodium Alginate Composite Hydrogel Membranes, *RSC Adv.*, 2024, **14**(1), 211–221, DOI: 10.1039/D3RA07554K.

67 S. Rojas, T. Baati, L. Njim, L. Manchego, F. Neffati, N. Abdeljelil, S. Saguem, C. Serre, M. F. Najjar, A. Zakhama and P. Horcajada, Metal–Organic Frameworks as Efficient Oral Detoxifying Agents, *J. Am. Chem. Soc.*, 2018, **140**(30), 9581–9586, DOI: 10.1021/jacs.8b04435.

68 A. Salek, M. Selmi, L. Njim, P. Umek, P. Mejanelle, F. Moussa, W. Douki, K. Hosni and T. Baati, Titanate Nanotubes as an Efficient Oral Detoxifying Agent against Drug Overdose: Application in Rat Acetaminophen Poisoning, *Nanoscale Adv.*, 2023, **5**(11), 2950–2962, DOI: 10.1039/d2na00874b.

69 L. Gazvoda, B. Višić, M. Spreitzer and M. Vukomanović, Hydrophilicity Affecting the Enzyme-Driven Degradation of Piezoelectric Poly-l-Lactide Films, *Polymers*, 2021, **13**(11), 1719, DOI: 10.3390/polym13111719.

70 Y. Y. Lee, A. Erdogan and S. S. C. Rao, How to Assess Regional and Whole Gut Transit Time With Wireless Motility Capsule, *J. Neurogastroenterol. Motil.*, 2014, **20**(2), 265–270, DOI: 10.5056/jnm.2014.20.2.265.

71 I. A. Edwards, A. G. Elliott, A. M. Kavanagh, J. Zuegg, M. A. T. Blaskovich and M. A. Cooper, Contribution of Amphipathicity and Hydrophobicity to the Antimicrobial Activity and Cytotoxicity of β-Hairpin Peptides, *ACS Infect. Dis.*, 2016, **2**(6), 442–450, DOI: 10.1021/acsinfecdis.6b00045.

72 R. Chen, S. Khormaee, M. E. Eccleston and N. K. H. Slater, The Role of Hydrophobic Amino Acid Grafts in the Enhancement of Membrane-Disruptive Activity of pH-Responsive Pseudo-Peptides, *Biomaterials*, 2009, **30**(10), 1954–1961, DOI: 10.1016/j.biomaterials.2008.12.036.

73 A. L. Mescher, Macrophages and Fibroblasts during Inflammation and Tissue Repair in Models of Organ Regeneration, *Regeneration*, 2017, **4**(2), 39–53, DOI: 10.1002/reg2.77.

74 J. M. Sorrell and A. I. Caplan, Fibroblast Heterogeneity: More than Skin Deep, *J. Cell Sci.*, 2004, **117**(5), 667–675, DOI: 10.1242/jcs.01005.

75 T. A. Wynn and K. M. Vannella, Macrophages in Tissue Repair, Regeneration, and Fibrosis, *Immunity*, 2016, **44**(3), 450–462, DOI: 10.1016/j.immuni.2016.02.015.

76 Y. Sambuy, I. De Angelis, G. Ranaldi, M. L. Scarino, A. Stammati and F. Zucco, The Caco-2 Cell Line as a Model of the Intestinal Barrier: Influence of Cell and Culture-Related Factors on Caco-2 Cell Functional Characteristics, *Cell Biol. Toxicol.*, 2005, **21**(1), 1–26, DOI: 10.1007/s10565-005-0085-6.

77 P. Hoffmann, M. Burmester, M. Langeheine, R. Brehm, M. T. Empl, B. Seeger and G. Breves, Caco-2/HT29-MTX Co-Cultured Cells as a Model for Studying Physiological Properties and Toxin-Induced Effects on Intestinal Cells, *PLoS One*, 2021, **16**(10), e0257824, DOI: 10.1371/journal.pone.0257824.

